Editors' choice

# Intraspecific variation and new morphological characters revealed by multimodal imaging analysis on the Late Cretaceous coleoid *Dorateuthis syriaca*

ALISON J. ROWE, ISABELLE KRUTA, LOÏC VILLIER, PIERRE GUERIAU, MARIE RADEPONT, OULFA BELHADJ, KATHARINA MÜLLER, ROMAIN JATTIOT, DIRK FUCHS, THOMAS CLEMENTS, SYLVAIN CHARBONNIER, and ISABELLE ROUGET

Rowe, A.J., Kruta, I., Villier, L., Gueriau, P., Radepont, M., Belhadj, O., Müller, K., Jattiot, R., Fuchs, D., Clements, T., Charbonnier, S., and Rouget, I. 2024. Intraspecific variation and new morphological characters revealed by multimodal imaging analysis on the Late Cretaceous coleoid *Dorateuthis syriaca*. *Acta Palaeontologica Polonica* 69 (4): 607–632.

The Cretaceous outcrops of Haqel, Hjoula (Cenomanian) and Sahel Aalma (Santonian) in Lebanon are renowned for their exceptional preservation of coleoid soft tissue in coeval shallow carbonate mud deposits and provide an unmatched opportunity to study many specimens of a single species, *Dorateuthis syriaca*. Despite being the most abundant coleoid from these localities, the taxon lacks clear, unambiguous diagnostic characteristics of both the gladius, and soft tissue anatomy. The absence of a defined character complex for the species has led to inconsistencies in the literature and the need for a reappraisal. This investigation represents the largest sample of *D. syriaca* studied with high-resolution, multi-imaging techniques, and has obtained a comprehensive morphological dataset of measurements on this key taxon. This has allowed us to refine some of the character states used to understand the phylogeny of coleoids. Furthermore, we have identified morphological characters that were previously undescribed for the genus, including suckers, axial nerves, and possible retractor muscles, as well as provided confirmation of the circulatory and excretory systems, and an Octobrachia-type digestive system. We also discount the presence of tentacles, tentacular pockets, and hooks within the arm crown, and we show that the species definition of *D. syriaca* is more complex than expected as our sample suggests intraspecific variability is present in the gladius. We strongly support the hypothesis that it was an 8-armed coleoid that was likely an active visual predator.

Key words: Coleoidea, Lagerstätte, multimodal imaging, soft tissue preservation, Lebanon.

*Alison J. Rowe [alison.rowe@sorbonne-universite.fr; ORCID: https://orcid.org/0009-0007-6356-6828], Isabelle Kruta [isabelle.kruta@sorbonne-universite.fr; ORCID: https://orcid.org/0000-0002-4485-541X], Loïc Villier [loic.villier@sorbonne-universite.fr; ORCID: https://orcid.org/0000-0003-4221-5176], Sylvain Charbonnier [sylvain.charbonnier@mnhn.fr; ORCID: https://orcid.org/0000-0003-2343-6897] and Isabelle Rouget [isabelle.rouget@mnhn.fr; ORCID: https://orcid.org/0000-0002-9673-0416], Centre de Recherche en Paléontologie – Paris (CR2P), Muséum national d'Histoire naturelle, Sorbonne Université, CNRS, 8 rue Buffon, CP 38, F-75005 Paris, France.*
*Pierre Gueriau [pierre.gueriau@hotmail.fr; ORCID: https://orcid.org/0000-0002-7529-3456], Institute of Earth Sciences, University of Lausanne, Géopolis, CH-1015 Lausanne, Switzerland; Université Paris-Saclay, CNRS, ministère de la Culture, UVSQ, MNHN, UAR 3461 Institut photonique d'analyse non-destructive européen des matériaux anciens (IPANEMA), 91192, Saint-Aubin, France.*
*Marie Radepont [marie.radepont@mnhn.fr; ORCID: https://orcid.org/0000-0002-9540-0247] and Oulfa Belhadj [oulfa.belhadj@mnhn.fr; ORCID: https://orcid.org/0009-0000-6939-3162], Centre de Recherche sur la Conservation – Paris (CRC), UAR 3224, MNHN, 36 rue Geoffroy St Hilaire, CP21, 75005 Paris, France.*
*Katharina Müller [katharina.muller@synchrotron-soleil.fr; ORCID: https://orcid.org/0000-0003-2386-7793], Université Paris-Saclay, CNRS, ministère de la Culture, UVSQ, MNHN, UAR 3461 Institut photonique d'analyse non-destructive européen des matériaux anciens (IPANEMA), 91192, Saint-Aubin, France.*
*Romain Jattiot [jattiot.romain@gmail.com; ORCID: https://orcid.org/0000-0003-0391-4636], Centre de Recherche en Paléontologie – Paris (CR2P), Muséum national d'Histoire naturelle, Sorbonne Université, CNRS, 8 rue Buffon, CP 38, F-75005 Paris, France; Biogéosciences, UMR6282, CNRS, Université Bourgogne, 6 Boulevard Gabriel, 21000 Dijon, France.*
*Dirk Fuchs [fuchs@snsb.de; ORCID: https://orcid.org/0000-0003-0648-1231], SNSB-Bayerische Staatssammlung für Paläontologie und Geologie, Richard-Wagner-Str. 10, 80333 Munich, Germany.*
*Thomas Clements [Clements.taph@gmail.com; ORCID: https://orcid.org/0000-0002-6563-4720], Friedrich-Alexander-Universität Erlangen-Nürnberg, Schloßplatz 4, 91054 Erlangen, Germany.*

Received 27 February 2024, accepted 19 July 2024, published online 19 December 2024.

# Introduction

In the Mesozoic fossil record, coleoid soft tissues are known from just a few key Lagerstätten (Donovan and Fuchs 2016). In the Jurassic, these include the Pliensbachian–Toarcian (Lower Jurassic) Ya Ha Tinda Lagerstätte (Alberta, Canada), the Toarcian (Lower Jurassic) Posidonia shales of Holzmaden (Germany), the Callovian (Middle Jurassic) deposits of La Voulte-sur-Rhône (France), the Oxfordian Clay Formation at Christian Malford (England), and the Kimmeridgian–Tithonian (Upper Jurassic) lithographic limestones of Solnhofen (Germany) (e.g., Wilby et al. 2004; Klug et al. 2005, 2015, 2021a, b; Fuchs 2007; Fuchs et al. 2007a, b, 2009, 2013, 2016a; Charbonnier 2009; Charbonnier et al. 2014; Kruta et al. 2016; Martindale et al. 2017; Marroquín et al. 2018; Hart et al. 2019; Muscente et al. 2019; Rowe et al. 2022; 2023). Coleoid soft tissues in the Cretaceous are famously known from the celebrated lithographic limestones of Lebanon (e.g., Fuchs and Weis 2009; Fuchs et al. 2009; 2016a; Jattiot et al. 2015). In this Lebanese Lagerstätte, coleoids are most abundant in three outcrops: Haqel, Hjoula (Cenomanian)—also referred to in the literature as Hâdjoula, Hâkel—and the Santonian-aged Sahel Aalma (Woodward 1883, 1896; Roger 1946; Fuchs 2006a, b; Fuchs and Weis 2009; Fuchs et al. 2009; Fuchs and Larson 2011a, b; Jattiot et al. 2015). The coleoid assemblage comprise ten genera from the octobrachian suborders Prototeuthina Naef, 1921, Teudopseina Roger, 1952, and Incirrata Grimpe, 1916 (Fuchs 2020); two of these genera, *Keuppia* Fuchs et al., 2009, and *Styletoctopus* Fuchs et al., 2009, are positioned as the oldest known representatives of the Incirrata (Fuchs et al. 2009; Fuchs 2020). From a taphonomic perspective, the soft tissue preservation surpasses that of the celebrated Solnhofen Limestones, in terms of morphological characters that are preserved (Fuchs 2006a, b; Fuchs et al. 2007a, b; Fuchs and Weis 2009). The prototeuthid *Dorateuthis syriaca* Woodward, 1883, is the most abundant coleoid in these Cretaceous-aged deposits (Fuchs and Larson 2011a). Despite this, the species lacks unambiguous diagnostic characteristics (Fuchs and Larson 2011a; Jattiot et al. 2015). The holotype has been noted to be poorly preserved (Fuchs 2006a), and many of its morphological characters are unclear and have been difficult to confirm using classical optical and UV photographic methods (Fuchs and Larson 2011a; Jattiot et al. 2015). The original species description by Woodward (1883) included some misinterpretations regarding the arm crown, fins, and gladius elements, which has contributed to ambiguity regarding the exact diagnosis (Roger 1946; Fuchs 2006a, 2007; Fuchs and Larson 2011a; Jattiot et al. 2015), and systematic placement (Naef 1922; Roger 1946; Bandel and Leich 1986; Fuchs 2006a, 2007; Jattiot et al. 2015). The current genus-level taxonomic description is outlined in Fuchs (2020); Fuchs and Larson (2011a) provided the species-level description. The morphological uncertainty noted for *D. syriaca* is widespread for Mesozoic coleoids and underpins the challenges inherent to the current systematic framework (e.g., Young and Vecchione 1996; Lindgren et al. 2004; Kruta et al. 2016; Sutton et al. 2016; Fuchs 2020; Whalen and Landman 2022). As such, there is no undisputed phylogeny that includes fossil and extant Cephalopoda.

*Dorateuthis syriaca* is known from three Lebanese localities, Hjoula, Haqel (Cenomanian), and Sahel Aalma (Santonian), making the range of the species occurrence ca. 9–10 Ma. Multiple individuals have been figured (e.g., Woodward 1883; Naef 1922; Roger 1946; Fuchs 2006a, b, 2007, 2020; Fuchs and Larson 2011a; Jattiot et al. 2015; Donovan and Fuchs 2016; Klug et al. 2021c) as *D. syriaca*, or identified as such in international collections (e.g., MNHN, NHMUK, BHI). As *D. syriaca* is represented by a greater number of individuals than any other coleoid species from the Lebanese localities, it provides an unprecedented opportunity to study the intraspecific variation, and possible anatomical variance related to taphonomic biases.

This study represents the most comprehensive analysis to date on a single fossil species that combines precise morphological measurements complemented by an array of non-destructive and multimodal imaging techniques. In light of new imaging methods, the holotype of *D. syriaca* and 53 additional figured and previously undescribed individuals were examined. The new data reveal previous anatomical misinterpretations, resolve a number of novel character states for phylogenetic reconstructions (Whalen and Landman 2022), identify undescribed intraspecific variation, and provide insight into the lifestyle of the species. The resulting qualitative and quantitative dataset provides the most comprehensive understanding to date of the morphology of *D. syriaca*.

*Institutional abbreviations*.—BHI, Black Hills Institute of Geological Research, Hill City, South Dakota, USA; CRC, Centre de Recherche sur la Conservation, Paris, France; iXRF, iXRF Systems, Austin, Texas, USA; MNHN, Muséum national d'Histoire naturelle, Paris, France; MNHNL, Musée national d'histoire naturelle, Luxembourg City, Luxembourg; MSNM, Museo Civico di Storia Naturale di Milano, Milan, Italy; NHMUK, Natural History Museum, London, UK; NHMW, Naturhistorisches Museum Vienna, Austria; NPL, The University of Texas at Austin, Jackson School Museum of Earth History, Austin, USA; SOLEIL, Synchrotron SOLEIL, Saint-Aubin, France.

# Geological setting

During the Cretaceous, modern-day Lebanon (Fig. 1) was part of a large system of shallow carbonate platforms that were positioned on the Arabian craton (northeastern section of Gondwana) in the southern Tethys (Ferry et al. 2007; Fuchs and Weis 2009; Fuchs et al. 2009; Audo and Charbonnier 2012). Within these warm waters, oscillations in relative sea-level deposited fine grained, laminated, organic-rich lithographic limestones in restricted, intra-shelf depressions (Fuchs 2006a, 2009; Ferry et al. 2007), and

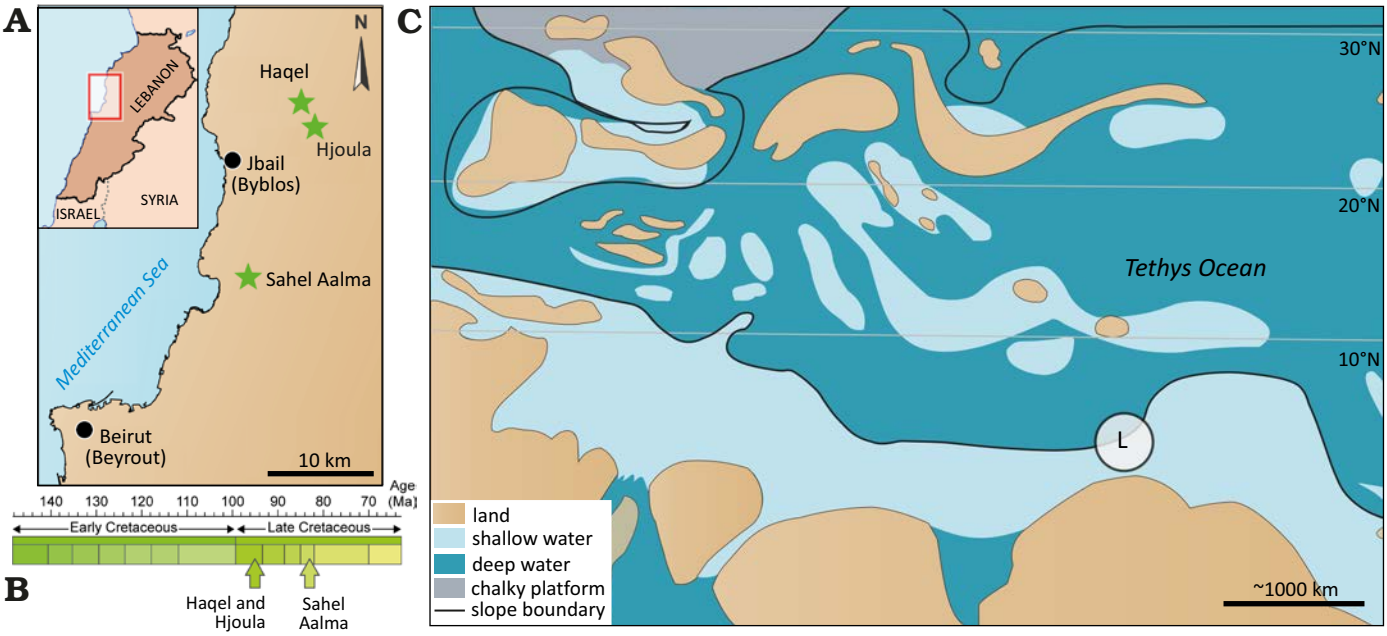


Fig. 1. Geographic location (**A**) and stratigraphic position (**B**). **C**. Simplified paleogeographic map of the Central Tethys during the Cretaceous. Modified from Forey et al. (2003) and Fuchs (200b). The encircled L reflects the palaeogeographic location of Lebanon.

formed the renowned Lagerstätte deposits of Hjoula, Haqel, and Sahel Aalma. Each deposit shows some variation in the depositional environment and fossil assemblage.

Biostratigraphic data indicates that the two older of the three sites, Haqel and Hjoula, formed somewhat contemporaneously in the late Cenomanian (Wippich and Lehmann 2004; Fuchs et al. 2009). Recent work by Lehmann et al. (2024), refined the biostratigraphy of Hjoula and determined the outcrop to be early late Cenomanian in age (Guerangeri Ammonoid Zone). Though Haqel and Hjoula are located geographically close to one another and share faunal similarities, they represent separate intra-shelf depressions (Fuchs et al 2009; Jattiot et al. 2015; George et al. 2024). Both outcrops are composed of highly fossiliferous lithographic limestones, though the sediments at Hjoula are more bituminous, have higher quantities of pyrite, and contain flint nodules (Swinburne and Hemelben 1994; George et al. 2024). Each deposit has a high diversity of fossil organisms, though Hjoula is dominated by crustaceans while Haqel is renowned for the abundance of small teleost fish (Forey et al. 2003; El Hosney et al. 2023; George et al. 2024). The chalky laminated limestones of Sahel Aalma are constrained to the Santonian (Ejel and Dubertret 1966; Fuchs 2006a), positioning it as ~10 My younger than the Cenomanian outcrops. In addition to the difference in lithology, Audo and Charbonnier (2013) identified taxa in the faunal assemblage consistent with a deeper depositional environment (Ferry et al. 2007; Fuchs et al. 2009; Fuchs and Larson 2011a; Audo and Charbonnier 2013), with a water depth most probably exceeding 150 m (Audo and Charbonnier 2013; George et al. 2024).

Today, these three outcrops are located within a belt of Cretaceous sediments (NE-SW) in northwest Lebanon and each bear the name of the corresponding neighbouring town. Combined, these three deposits preserve exceptional faunal assemblages, including Late Cretaceous fishes (Forey et al. 2003), arthropods (Roger 1946; Audo and Charbonnier 2013; Charbonnier et al. 2017; Audo et al. 2021), annelids (Bracchi and Alessandrello 2005), echinoderms (Reich 2004), as well as coleoid, ammonoid, and nautiloid cephalopods (Wippich and Lehmann 2004; Klug et al. 2021b). The Sahel Aalma outcrop is no longer accessible due to urban development (George et al. 2024) therefore, most samples in this study are from the two Cenomanian sites. The coleoid fauna from these deposits were subject to authigenic mineralization and phosphatization of the soft tissues, which has preserved fine anatomical detail in many specimens (Fuchs et al. 2009; Fuchs and Weis 2009; Fuchs and Larson 2011a, b). Phosphatization is quite selective as some tissues (e.g., the muscular mantle) commonly recorded, while others (e.g., digestive organs) are not preserved to the same extent (Clements and Gabbott 2022).

# Material and methods

*Material*.—The sample of *Dorateuthis syriaca* used in this study includes 54 individuals selected from a larger group of 90 individuals, chosen as they preserved a generally complete gladius upon which diagnostic observations could be made. The individuals included are reposited in the collections of the MNHN (n = 11); NHMUK (n = 2); BHI (n = 29); NPL (n = 1); NHMW (n = 1); MNHNL (n = 1); MSNM (n = 4), as well as 5 individuals made available through photographs from a database of co-author DF. The provenance of the individuals is recorded as Haqel (n = 3),

Hjoula (n = 36), and Sahel Aalma (n = 8). The remaining 7 individuals are also from the Lebanese Lagerstätten, though the precise provenance is not recorded. Specimens are preserved either in dorsal, ventral, slight dorso-lateral, or slight ventro-lateral view (Table 1, SOM: table 1, Supplementary Online Material available at http://app.pan.pl/SOM/app69-Rowe_etal_SOM.pdf). Specimens preserved in fully lateral view were excluded from this study.

*Methods*.—In order to retrieve as much anatomical information as possible from the sample for systematic, phylogenetic and palaeoecological purposes, a series of individuals was subjected to multimodal imaging. The type of imaging utilized was based on availability and preservation of the specimens (Table 2). These non-destructive methods range from photography in natural light, to techniques that exploit different physical properties across several regions of the electromagnetic spectrum (e.g., visible, UV, X-rays).

*Optical photography and Reflectance Transformation Imaging (RTI)*: High resolution photographs of 11 individuals were taken in natural light at the MNHN using a Nikon D800 camera with either a 100 mm or 50 mm Macro lens depending on the detail required. Ten individuals were imaged with RTI at the MNHN, Paris, France following the set up outlined in Béthoux et al. (2016). The photographic equipment included a FlyDome RTI set up (light dome, control box and reflective black hemispheres) and Canon EOS 5D Mark III digital camera, which was coupled with either a 100 mm or 50 mm Canon macro lens (without polarizing filters). The camera lens used, and size of the dome (either 30 cm, or 50 cm in diameter), depended on the size of the individual fossil. Within the dome, 54 LED lights were positioned on three rigid rings that encircled the internal surface at different latitudes. These lights provided the illumination for the acquisition. The illumination sequence and triggering of the camera were automated and regulated by a dedicated control box, which produced a set of 54 photographs. Some of these individual photographs were used as illustrations in figures (e.g., Figs. $3A_3$–$A_5$, $4B_1$, $C_1$, 11B, $12B_1$, $14A_2$–$A_4$, $15A_1$, $A_3$, C, 16A, B). Each of the photographic sets were also used to compute the RTI files using RTIbuilder software (using the HSH fitter). Reflective black hemispheres placed adjacent to the fossils during acquisition recorded the position of the LED light source during computation.

*UV photography*: Two types of images were collected under UV illumination. Classical UV photography was carried out on 11 individuals at the MNHN using a Nikon D800 and either a 100 mm or 50 mm Macro lens with the addition of two Fluotest Forte lamps, enabling luminescence in the long wave range at 366 nm. Multispectral UV-visible-near infrared luminescence imaging was performed on 3 individuals at the UAR 3461 IPANEMA, Saint-Aubin, France. Luminescence, and reflection images were collected in various spectral ranges using an in-house setup consisting of a low-noise 4.2-megapixel CMOS camera (ORCA-Flash4.0 LT PLUS, Hamamatsu, Japan) with high sensitivity from 350–900 nm, fitted with a UV-VIS-IR 60 mm 1:4 Apo Macro lens (CoastalOptics) and filter wheel holding eight interference band-pass filters (Semrock) to collect images in eight spectral ranges from 472–935 nm. Illumination was provided by 16 LED lights ranging from 365–770 nm wavelength (CoolLED pE-4000), coupled to a liquid light-guide fitted with a fibre-optic ring light-guide. One of the resulting greyscale images is shown in Fig. $11A_2$.

Table 1. Synthesis of the preserved orientation of the individuals and how the gladius measurements were obtained.

| | Number of specimens |
|---|---|
| Preserved orientations | (n = 54) |
| dorsal/ventral (part and counterpart) | 8 |
| dorsal | 11 |
| ventral | 25 |
| dorso/ventral lateral | 5 |
| dorso-and-ventral lateral (part and counterpart) | 1 |
| unclear | 4 |
| Measurement acquisition (gladius) | |
| directly measured | 19 |
| straightened | 33 |
| composite | 2 |

*X-ray fluorescence analyses*: The elemental composition and associated distributions were determined for 7 individuals using micro-X-ray fluorescence (μXRF) mapping. Due to availability and location of the specimens, 3 different μXRF scanners were used during the project. Synchrotron-based μXRF major-to-trace elemental mapping was performed on 5 of these individuals at the PUMA Beamline of the SOLEIL Synchrotron, Saint-Aubin, France using a monochromatic beam of 18.2 keV, selected for excitation of K-lines from phosphorus to zirconium and L-lines from cadmium to uranium. The incoming X-ray beam was focused using Kirkpatrick-Baez mirrors down to a spot size of ~10×5 $\mu m^2$ (H×V, full width at half maximum). XRF was collected using a SiriusSD silicon drift detector (SGX Sensortech Ltd, 100 $mm^2$ active area) oriented at 90° to the incident beam, in the horizontal plane, and 30° to the sample. Two-dimensional spectral images, i.e., images for which each pixel is characterized by a full XRF spectrum, were collected on the fly (Leclercq et al. 2015) over the individuals at a 85–200 μm lateral resolution with a 40–80 ms dwell time (effective counting time was 90% of the dwell time) depending on the samples.

Laboratory-based μXRF major-to-minor elemental mapping was conducted on 2 individuals using a M6 Jetstream Bruker XRF (Alfeld et al. 2013) at the UAR 3224 Centre de Recherche sur la Conservation, MNHN, CNRS, Paris, France (one of these specimens was also imaged at the SOLEIL Synchrotron). This instrument is equipped with a rhodium anode, used at 50 kV and 600 μA, with a 100 μm thick beryllium window. Polycapillary optics were used to focus the X-ray beam. The X-ray detector was a 60 $mm^2$ SDD

Table 2. Summary of the acquisition parameters for each of the specimens figured. Note, this does not reflect all the individuals in the study sample (see SOM). The abbreviations noted in the Acquisition / Equipment column indicate the person and/or institution associated with the acquisition: AJR – Alison J. Rowe, DF – Dirk Fuchs, LC, Lilian Cazes; OB, Olivier Béthoux.

| Specimen | Imaging type | Acquisition / Equipment | Illumination/ excitation | Beam size/ full field | Acquisition/ dwell time | Figures |
|---|---|---|---|---|---|---|
| BMNH C5017 (holotype) | µXRF | CRC, M6 Jetstream Bruker XRF | Rhodium anode, 50 kV | 100 µm | 2000 ms | 3, 8 |
| | RTI | MNHN (OB) / FlyDome RTI set up, Canon EOS 5D Mark III digital camera | – | – | – | 3, 4 |
| | photograph (UV light) | MNHN (LC) / Nikon D800, Fluotest Forte lamps | 366 nm | – | – | 3 |
| BHI 2201 | photograph (natural light) | photographs provided (DF) | – | – | – | 4 |
| MNHN.F.A88588 | µXRF | SOLEIL / PUMA Beamline | monochrome 18.2 KeV | – | – | 8, 17 |
| | RTI | MNHN (AJR) / FlyDome RTI set up, Canon EOS 5D Mark III digital camera | | | | 4 |
| BHI 2205 | photograph (natural light) | provided (DF) | – | – | – | 2 |
| | µXRF | iXRF, Atlas X microXRF spectrometer | – | – | – | 8 |
| | photograph (UV light) | provided (DF) | – | – | – | 17 |
| MSNMi 24800 | photograph (natural light) | provided (DF) | – | – | – | 4 |
| BHI 2229 | photograph (UV light) | provided (DF) | – | – | – | 9 |
| BHI 5779 | photograph (UV light) | provided (DF) | – | – | – | 9 |
| BHI 2203 | photograph (UV light) | provided (DF) | – | – | – | 10 |
| NHMW 1998z0105/0000 | photograph | Lukeneder and Harzhauser 2004: pl. 1.1 | – | – | – | 11 |
| | photograph | Jattiot et al. 2015: fig. 12.3 | – | – | – | 10 |
| MNHN.F.A88589 | µXRF | CRC, M6 Jetstream Bruker XRF | Rhodium anode, 50 kV | 180 µm | 500 ms | 8 |
| | UV–visible–near infrared multispectral imaging | IPANEMA Platform | 385 nm (spectral range), 514 nm (illumination) | – | 30000 ms | 11 |
| | photograph (natural light) | MNHN (LC) / Nikon D800 | – | – | – | 14 |
| | RTI | MNHN (AJR) / FlyDome RTI set up, Canon EOS 5D Mark III digital camera | – | – | – | 14, 15, 16 |
| | photograph (UV light) | MNHN (LC) / Nikon D800, Fluotest Forte lamps | 366 nm | – | – | 17 |
| MNHN.F.A50396 | RTI | MNHN (AJR) / FlyDome RTI set up, Canon EOS 5D Mark III digital camera | – | – | – | 11 |
| BHI 2222 | photograph (natural light) | provided (DF) | – | – | – | 13 |
| MNHN.F.A50400 | RTI | MNHN (AJR) / FlyDome RTI set up, Canon EOS 5D Mark III digital camera | – | – | – | 13 |
| MNHN.F.R06746 | RTI | MNHN (AJR) / FlyDome RTI set up, Canon EOS 5D Mark III digital camera | – | – | – | 15 |
| | photograph (UV light) | MNHN (LC) / Nikon D800, Fluotest Forte lamps | 366 nm | – | – | 15 |
| BHI 2213 | photograph (natural light) | provided (DF) | – | – | – | 15 |
| MNHN.F.A88590 | RTI | MNHN (AJR) / FlyDome RTI set up, Canon EOS 5D Mark III digital camera | – | – | – | 16 |
| BHI 2219 | photograph (UV light) | provided (DF) | – | – | – | 16 |
| NPL 52121 | photograph (natural light) | provided (DF) and NPL | – | – | – | 11 |
| BHI 2212 | photograph (natural light) | provided (DF) | – | – | – | 17 |
| BHI 2227 | photograph (natural light) | provided (DF) | – | – | – | 17 |

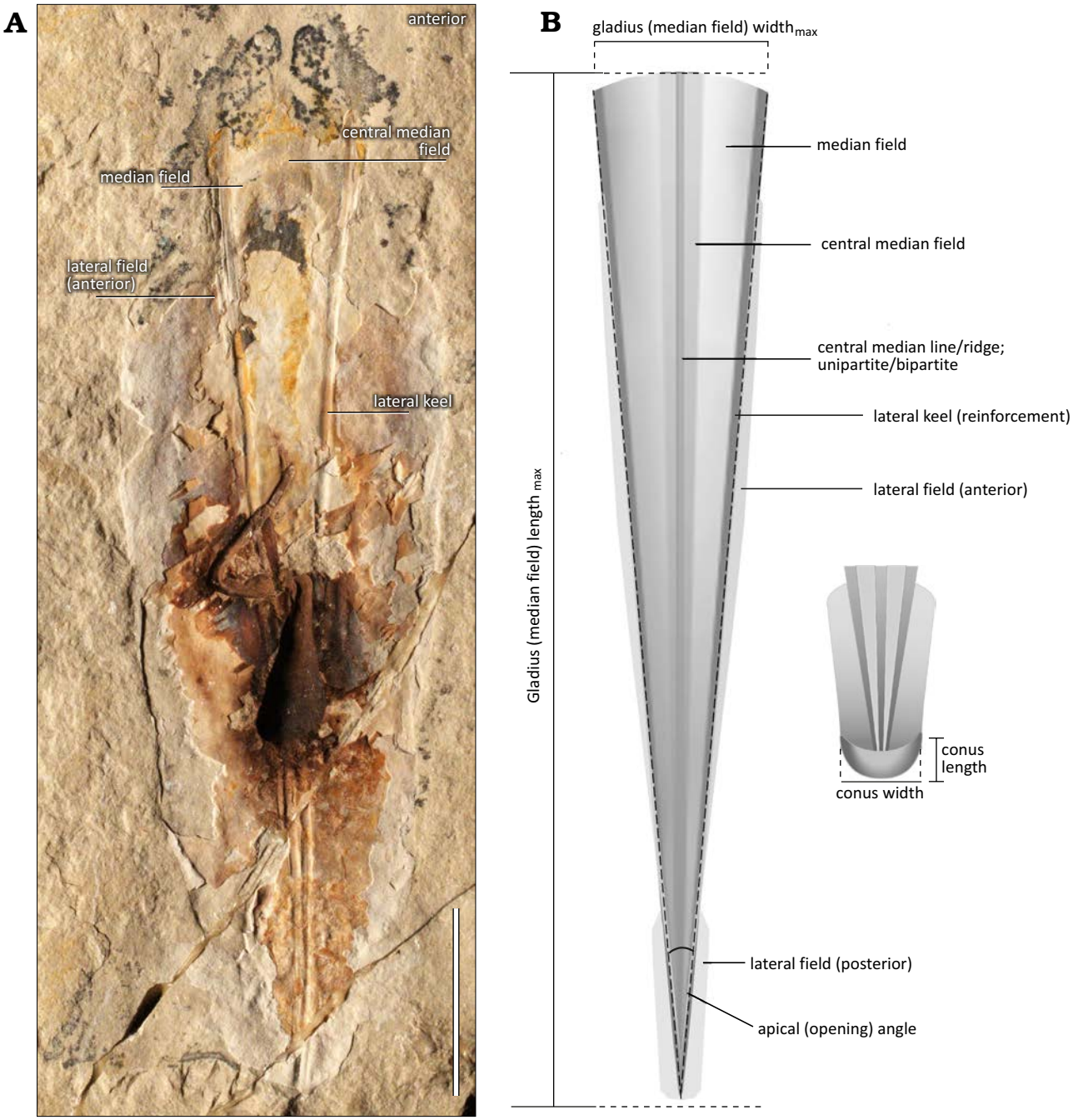


Fig. 2. **A**. Photograph of coleoid cephalopod (BHI 2205) from Cenomanian of Hjoula, Lebanon, showing the gladius. Scale bar 20 mm. **B**. Hypothesized illustration of plesioteuthid coleoid *Dorateuthis syriaca* Woodward, 1883, gladius adapted from Fuchs (2006b, 2007, 2016, 2020) and Fuchs and Larson (2011a). The gladius has the triangular-shaped median field and funnel-like conus characteristic of the suborder Prototeuthina. Pronounced lateral keels and a bipartite median ridge extend from the anterior to posterior margins; a median keel is not present in *Dorateuthis* (Fuchs 2020). The anterior margin is slightly convex. The apical angle is <12°. Both the observed anterior and posterior, lateral fields are indicated in this illustration. Not to scale.

with a Peltier cooler, which 4096 channels were divided into 40 keV with a maximum count rate of 275 kcps. For the targets MNHN.F.A88589 and the holotype BMNH C5017, the beam presented a diameter of 180 and 100 µm respectively, a corresponding step size of 180 and 100 µm, and a dwell time of 500 and 2000 ms. The targets were placed horizontally at a working distance of 15 mm and 12 mm respectively. Data were processed with the instrument software developed by Bruker. Additional elemental mapping was conducted on 1 individual at iXRF Systems, Austin, TX, USA using an Atlas X micro-XRF spectrometer equipped with a 5-micron polycapillary source. This instrument is equipped with a rhodium anode, used at 50 kV and 1000 µA. The simulated pixel size was 10 µm with a per pixel point dwell time of 100 ms. Spectral images were collected without a filter in a vacuum environment.

Elemental distributions presented herein are shown as false-colour RGB overlays of 3 elemental distributions (Cu/

Y/P, and Sr/Ti/Fe), corresponding with integrated intensities from the main XRF peaks (Figs. 3A$_1$, A$_2$, 8). Overlays from SOLEIL Synchoroton and iXRF Systems were generated using PyMCA data-analysis freeware (SOLEIL Synchrotron, iXRF Systems) and are presented in logarithmic scale (Solé et al. 2007); Overlays from the CRC are in linear scale.

*Measurements*.—As a basis for the systematic revision, we used the diagnostic characteristics for *Dorateuthis* from Fuchs (2020), which provides a range of measurements for the genus, and the indices used to describe the various characters used in this reassessment. All measurements in this study were obtained using FIJI ImageJ software (Schindelin et al. 2012). Following common terminology, body length refers to the cumulative measurements of the mantle, head, and arms (posterior-most tip of the mantle to anterior-most tip of the longest preserved arms), while mantle length reflects the length of the mantle only.

Initially, each individual was evaluated to determine if the gladius was complete or preserved in such a way that diagnostic measurements could be obtained. This was carried out either on the fossil, or by analysing photographs of the individual (UV or natural light). Two key diagnostic measurements include the width and length of the gladius (Fig. 2 and SOM: table 2). Additional measurements and observations on other gladius elements (e.g., apical angle and reinforcements) were then obtained (Fig. 2 and SOM: table 2 for measurements and tables 3, 4 for indices and characters respectively). Arm measurements were gathered for 22 individuals. Where the arms were visible, and the position of the eye could be determined, arms were measured from the central line of the eye, tracing the curve, to the anterior-most arm tip (SOM: table 2). This method followed the parameters for Octobrachia outlined in Nixon (2011: fig. 3). The arm pairs of *Dorateuthis* vary in length (Fuchs 2020) so where arm lengths have been used as indices, the maximum lengths were utilized. The entire sample was evaluated for the presence and configuration of suckers, cirri, and the arrangement of the arm crown.

Eyes were not visible in the holotype, so the length of the cephalic cartilage was used as a proxy for their diameter. Where the eyes and lenses were preserved, their maximum and minimum diameters were measured. Soft tissues and organs visible in the various imaging methods were recorded.

# Systematic palaeontology

## Subclass Coleoidea Bather, 1888

## Superorder Octobrachia Haeckel, 1866

## Suborder Prototeuthina Naef, 1921

## Family Plesioteuthidae Naef, 1921

## Genus *Dorateuthis* Woodward, 1883

*Type species*: *Dorateuthis syriaca* Woodward, 1883, by monotypy; upper Santonian, Sahel Aalma, Lebanon.

*Included species*: *Dorateuthis syriaca* Woodward, 1883, is the only species that can be assigned with certainty. *Neololigosepia stahleckeri* Reitner & Engeser, 1982, and *Maioteuthis morroensis* Reitner & Engeser, 1982 (Barremian, Cape Verde Islands); *Plesioteuthis* sp. of Engeser and Reitner (1985) and *Maioteuthis damesi* Engeser & Reitner, 1985 (Aptian, Heligoland, Germany); *Plesioteuthis arcuata* von der Marck, 1873 (Campanian, Germany), and *Plesioteuthis maestrichtensis* Binkhorst van den Binkhorst, 1861 (Maastrichtian, The Netherlands) are all assigned to this genus based on their narrow gladius and continuous lateral keels, though they are represented by poorly preserved individuals.

*Emended diagnosis* (modified from Fuchs 2020).—Very small to medium-sized (mantle length <50–400 mm). Gladius very slender to slender (gladius width$_{max}$ to gladius length 0.05–0.19). Central reinforcements variable; median line or ridge but no keel; uni- or bipartite. Median field very slender (apical angle <12°), median field area very large (median field area to gladius area >0.8). Anterior margin slightly convex. Lateral keels (reinforcements) pronounced, present from anterior to posterior margins. Lateral fields variable: absent, anterior (field length to gladius length$_{max}$ ratio 0.8–0.9), posterior (field length to gladius length$_{max}$ ratio ~0.3); narrow when present. Conus ventrally closed (conus length$_{max}$ to gladius length$_{max}$ ratio 0.03–0.05). Arm length moderate (arm length to mantle length ratio ~0.5); elongated dorsal pair. Cephalic cartilage ring-shaped in lateral view. Fins anteriorly rounded, "oar-shaped".

*Stratigraphic and geographic range*.—Barremian (Lower Cretaceous)–Maastrichtian (Upper Cretaceous): Lebanon, northern Germany, Cape Verde Islands, the Netherlands.

### *Dorateuthis syriaca* Woodward, 1883

Figs. 2–4, 8–19.

1878 *Sepialites*; Fraas 1878: 346.
1883 *Dorateuthis syriaca* n. sp.; Woodward 1883: 1–5, pl. 1.
1888 *Curculionites senonicus*; Kolbe 1888: 135, pl. 11, fig. 8.
1896 *Sepialites*; Woodward 1896: 231.
1922 *Dorateuthis syriaca* Woodward, 1883; Naef 1922: 118.
1922 "*Plesioteuthis fraasi*" Woodward, 1896; Naef 1922: 133, fig. 50.
1922 "*Sepialites sahil–almae*" O. Fraas, 1878; Naef 1922: 134, fig. 49c.
1943 *Sepialites sahil almae*; Klinghardt 1943: 12, fig. 8.
1946 *Leptoteuthis syriaca* Woodward, 1883; Roger 1946: 14, pl. 4: 5, 6, pl. 9: 1, 2.
1986 *Dorateuthis sahilalmae* Naef, 1922; Engeser and Reitner 1986: 3, fig. 1, pl. 1: 1.
1986 ?*Dorateuthis* sp.; Engeser and Reitner 1986: 4, pl. 1: 2.
1987 *Sepialites sahilalmae* (O. Fraas) Naef, 1922; Riegraf 1987: 97.
1988 *Dorateuthis sahilalmae* Naef, 1922; Engeser 1988: 43.
2006a *Dorateuthis* cf. *syriaca* Woodward, 1883; Fuchs 2006b: 7, fig. 4, pls. 1–3.
2006b *Dorateuthis sahilalmae*; Fuchs 2006a: pls. 17h, 22f.
2007b *Dorateuthis syriaca* Woodward, 1883; Fuchs et al. 2007b: 246.
2007b *Dorateuthis sahilalmae* Naef, 1922; Fuchs et al. 2007b: 246.
2007 *Dorateuthis syriaca* Woodward, 1883; Fuchs 2007: 64, fig. 4.
2007 ?*Dorateuthis sahilalmae* Naef, 1922; Fuchs 2007: 64.
2011a *Dorateuthis syriaca* Woodward, 1883; Fuchs and Larson 2011a: 237, figs. 2–6, 7.5, 8.
2015 *Dorateuthis syriaca* Woodward, 1883; Nixon 2015: 8, fig. 6a, c, d.

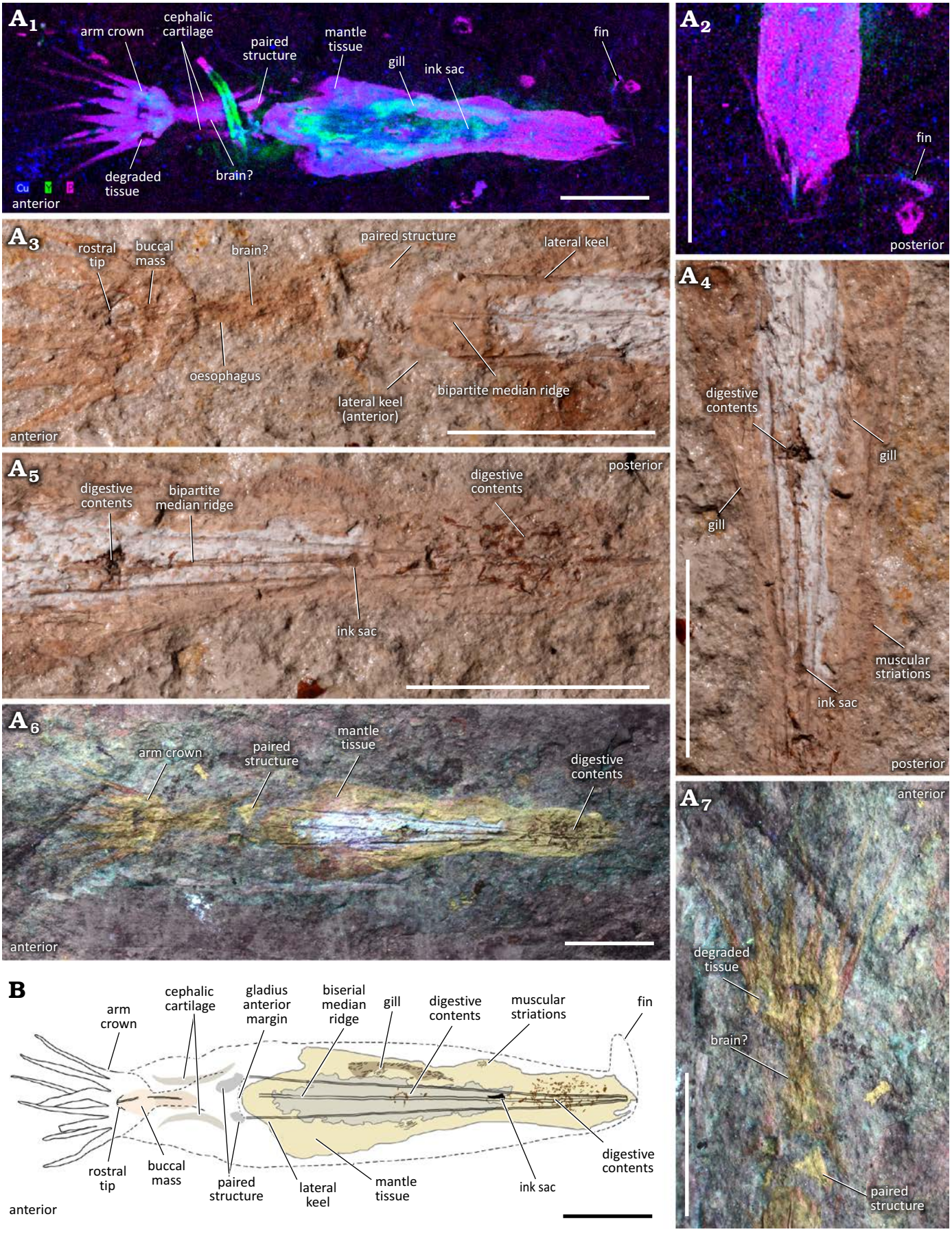
A1
arm crown
cephalic cartilage
paired structure
mantle tissue
gill
ink sac
fin
degraded tissue
brain?
anterior
A2
fin
posterior
A3
rostral tip
buccal mass
brain?
paired structure
lateral keel
oesophagus
lateral keel (anterior)
bipartite median ridge
anterior
A4
digestive contents
gill
gill
muscular striations
ink sac
posterior
A5
digestive contents
bipartite median ridge
digestive contents
posterior
ink sac
A6
arm crown
paired structure
mantle tissue
digestive contents
anterior
A7
anterior
degraded tissue
brain?
paired structure
B
arm crown
cephalic cartilage
gladius anterior margin
biserial median ridge
gill
digestive contents
muscular striations
fin
rostral tip
buccal mass
paired structure
lateral keel
mantle tissue
ink sac
digestive contents
anterior

← Fig. 3. **A**. The holotype BMNH C5017 of plesioteuthid coleoid *Dorateuthis syriaca* Woodward, 1883, from the upper Santonian of Sahel Aalma, Lebanon, as illustrated by multiple non-destructive imaging techniques. $A_1$, μXRF overlay of copper (blue), yttrium (green) and phosphorous (pink) distributions over the entire individual; $A_2$, rotated close-up of the posterior section with the fin outline visible on the right; $A_3$–$A_5$, individual images from the RTI stack showing the anterior part of the body, head, and arm crown ($A_3$), the posterior part of the body ($A_4$), and the central part of the body ($A_5$); $A_6$, $A_7$, UV photographs of the entire individual ($A_6$) and the anterior part of the body, head, and arm crown ($A_7$). **B**. Hypothesized illustration of the holotype (Jessica Gardner). The Y-enriched elongate feature in $A_1$ is not considered part of the individual, but part of a contemporaneous organism. Scale bars 10 mm.

2015 *Dorateuthis syriaca* Woodward, 1883; Jattiot et al. 2015: 152, figs. 4–6, 10, 11, 12.1–3, 13.2–3, 14.

2016 *Dorateuthis syriaca* Woodward, 1883; Donovan and Fuchs 2016: 20, figs. 12–15.

2016b *Dorateuthis syriaca*; Fuchs et al. 2016a: 438, figs. 1, 9.

2018 *Dorateuthis syriaca* Woodward, 1883; Gueriau et al. 2018: 985, fig. 5.

2020 *Dorateuthis syriaca* Woodward, 1883; Fuchs 2020: 11, fig. 3.

2021c *Dorateuthis syriaca* Woodward, 1883; Klug et al. 2021c: 7, fig. 5.

*Holotype*: BMNH C5017, original of Woodward (1883: pl. 1).

*Type locality*: Sahel Aalma, Lebanon.

*Type horizon*: Upper Santonian, Upper Cretaceous.

*Description*.—Redescription of the holotype.—It is preserved in ventral view (Fig. 3). The body length (the posterior mantle margin to the anterior tip of the arms) is ~68 mm. The length of the gladius is ~40 mm and corresponds with the length of the mantle. It has a triangular median field and convex (Fig. $3A_3$, $A_6$) anterior margin (~4 mm wide). The gladius has well defined lateral reinforcements (keels) and a central bipartite ridge. All are continuous from the anterior to the posterior margin (Fig. $3A_6$, B). The apical angle is 6.3°. There is no evidence of a central median field encompassing the individual's bipartite ridge. There is no evidence of lateral fields, hyperbolar zones or a conus.

μXRF elemental mapping and UV photography enables the most precise assessment of arm length to date. The holotype has eight tapered arms (Fig. $3A_1$, $A_7$, B). Six appear complete and range from 18–21 mm in length. Two lack their distal sections and have a preserved length of 15 and 17 mm. Using the index (arm length $_{max}$ to gladius length) outlined in Fuchs (2020) the arms are "moderate" in size (a ratio of 0.53). The preserved diameter of seven of the arm bases varied between 0.5 and 1.4 mm. The arm with the smallest diameter (0.5 mm) is partially obscured by another arm, and therefore the original diameter was likely larger. There is no evidence of an additional tentacular pair, or any associated hooks that were noted in the original description by Woodward (1883). No suckers or cirri were observed.

μXRF elemental mapping reveals the cephalic cartilage (Fig. $3A_1$), which is enriched in phosphorus and observed as two concave, semi-circular traces that flank the oesophagus in an anterior-posterior orientation. The cartilage is about 9 mm in length and is positioned between the posterior margin of the arm crown and the anterior lateral keels. The structures have a larger medial separation than is normally observed in dorsal view, and do not have the "pear-shape" associated with ventral view (Fuchs and Larson 2011a: fig. 4), therefore we interpret what is preserved to be a central slice (Fig. $3A_1$). The length of the cephalic cartilage was used as a proxy for eye diameter for the holotype. The ratio between the eyes and the gladius length (diameter$_{max}$ to gladius length) is ~0.23. The cephalic cartilage flanks a mass of soft tissue that corresponds with the oesophagus and possibly the brain or optic lobes. The position of the cephalic cartilage is inconsistent with the eye position supposed by Woodward (1883). Indeed, imaging reveals their interpretation reflects degraded tissue at the base of the arm crown (Fig. $3A_1$, $A_7$). Small protrusions, visible in the UV photographs and elemental maps, are positioned anteriorly to the lateral keels and likely represent soft tissue (Fig. $3A_1$, $A_3$, $A_6$, $A_7$). It is possible that these

Table 3. Synthesis of the size ranges (in mm) and mean measurements observed in the *Dorateuthis syriaca* sample. Genera-level values (Fuchs 2020) are provided for reference.

| Number (n) of individuals | Range | Mean | Standard error |
|---|---|---|---|
| Gladius width (n = 54) | 2.2–31.8 | 13.8 | 0.7 |
| Gladius length (n = 54) | 40–241 | 111.9 | 4.8 |
| Gladius length (genera value, Fuchs 2020) | 201–400 | – | – |
| Indices: gladius width (n = 54) | 0.05–0.17 | 0.12 | 0.00 |
| Indices: gladius width (genera value, Fuchs 2020) | 0.10–0.19 | – | – |
| State: gladius width (n = 54); very slender (n = 7), slender (n = 47) | | | |
| Apical angle (n = 54) [°] | 2.6–9.6 | 6.9 | 0.2 |
| Indices: apical angle (genera value, Fuchs 2020) [°] | <12 | – | – |
| Indices: posterior lateral field width (n = 5) | 0.37–0.67 | 0.5 | 0.05 |
| Indices: posterior lateral field length (n = 5) | 0.17–0.42 | 0.3 | 0.05 |
| Indices: anterior lateral field length (n = 7) | 0.7–0.9 | 0.8 | 0.02 |
| Indices: arm length (n = 23) | 0.35–0.89 | 0.6 | 0.03 |
| Indices: arm length (genera value, Fuchs 2020) | 0.4–0.8 | ~0.5 | – |
| Indices: eye diameter (n = 18) | 0.13–0.25 | 0.17 | 0.01 |
| Indices: buccal mass (n = 30) | 0.05–0.19 | 0.13 | 0.01 |

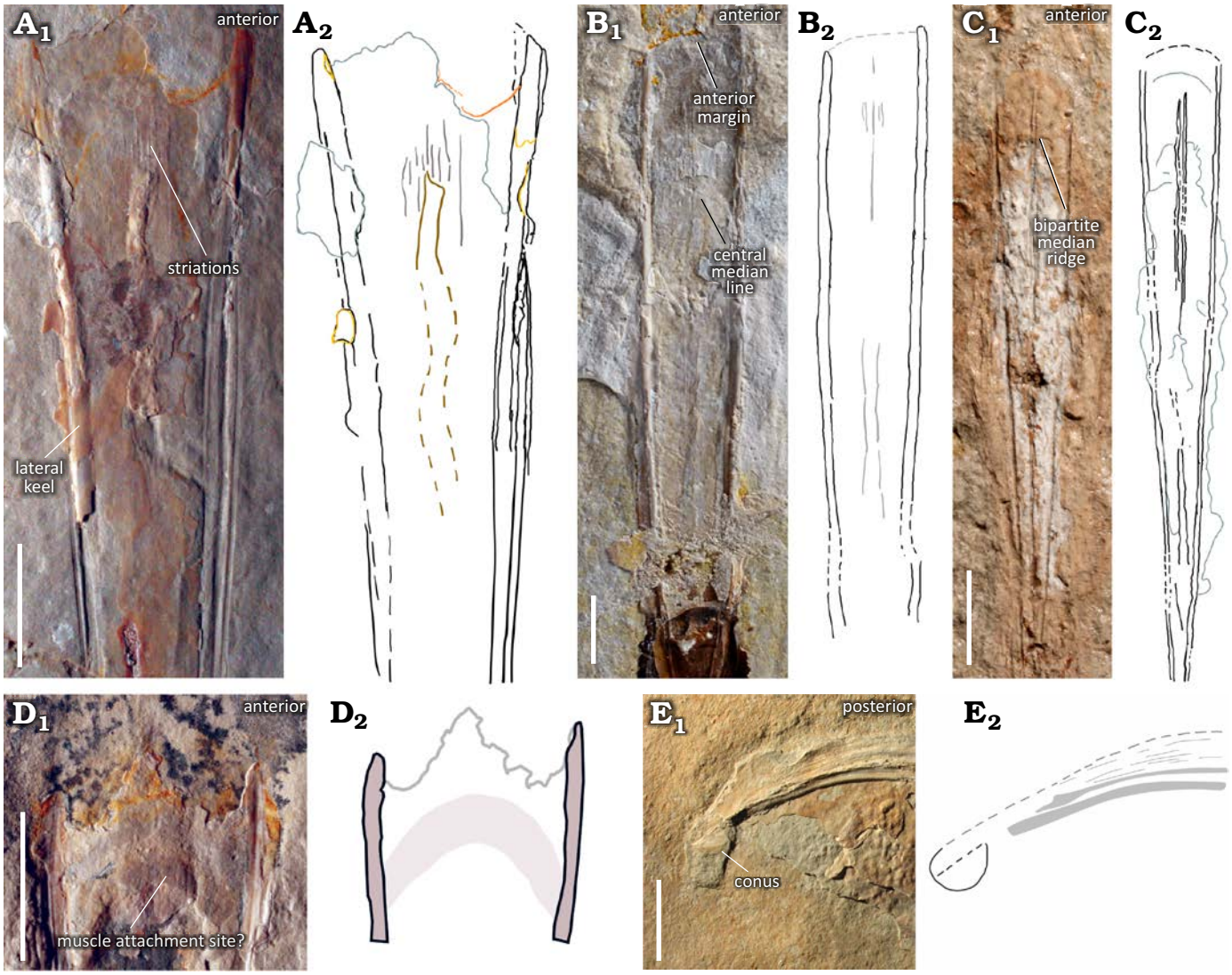


Fig. 4. Gladius morphologies observed in plesioteuthid coleoid *Dorateuthis syriaca* Woodward, 1883, from the Upper Cretaceous of Lebanon, showing the characteristic triangular-shaped median field, slightly convex anterior margin, and median reinforcement types. **A**. BHI 2201 (Hjoula, Cenomanian). **B**. MNHN.F.A88588 (Hjoula, Cenomanian). **C**. BMNH C5017, holotype (Sahel Aalma, Santonian). These median reinforcements take the form of a central median field that may have longitudinal striations (A, B). A central median line (B) or ridge (C) is also observable in the sample; these can be unipartite (B) or bipartite (C), and are observed with a central median field (B), and without (C). **D**. BHI 2205 (Hjoula, Cenomanian), showing a semi-circular imprint that possibly reflects a muscle attachment site. **E**. MSNMi 24800 (Hjoula, Cenomanian), shows a ventrally closed conus, characteristic of Prototeuthina. $A_1$–$E_1$, photographs ($A_1$, $D_1$, $E_1$, natural light; $B_1$, $C_1$, individual RTI images); $A_2$–$E_2$, interpretative drawings. Scale bars 10 mm.

represent posterior salivary glands or are the remnants of retractor musculature. Two areas of digestive contents are visible (Fig. $3A_4$, $A_6$, B). The anterior-most area was originally described as an ink sac (Woodward 1883: pl. 1), however, our multimodal imaging reveals these structures are in fact digestive remnants. A random sampling of fragment sizes in these two digestive assemblages shows that the anterior remains are roughly 0.2–0.4 mm in length, while those in the posterior section have larger components (approximately 0.2–1.2 mm). A small ink sac is more posteriorly located (Fig. $3A_4$, B). RTI and μXRF mapping also reveal faint imprints of what we interpret to be elongate gill lamellae and a posterior fin (Fig. $3A_1$ to $A_5$). The contours of the fin revealed by elemental mapping (Fig. $3A_2$) resemble the "oar-shaped" characteristic described for *Dorateuthis* (Fuchs 2020). As fins are otherwise unknown in individuals from Sahel Aalma (Fuchs and Larson 2011a), this represents the only known coleoid fin tissue preserved from this locality for this species.

*Redescription of* Dorateuthis syriaca.—*Size*: The diagnostic mantle length for *Dorateuthis* is 201–400 mm (Fuchs 2020), which is categorised as "medium" in size. These sizes were defined by Fuchs (2020: 7) as "very small" (<50 mm) small (50–200 mm), "medium" (201–400 mm), "large" (401–1500 mm), and "very large" (>1500 mm). The mean mantle length in this study is smaller (~112 mm, Tables 3 and 4), however, one of our measured samples, MNHN.F.A50402 (Jattiot et al. 2015: fig. 4.3), did fall within the range for the "medium" sized mantle length (241 mm). The rest are either "small" (~93%, n = 50), or "very small" (6%, n = 3). The body length

Table 4. Synthesis of the gladius length (in mm) observed in the *Dorateuthis syriaca* sample. Genera-level values (Fuchs 2020) are provided for reference.

| | Very small | | Small | | Medium | |
|---|---|---|---|---|---|---|
| | sample (n = 50) | genera | sample (n = 3) | genera | sample (n = 1 ) | genera |
| Range | 67.6–175.1 | <50 | 40–47 | 50–200 | 241 | 201–400 |
| Mean | 113.4 | – | 44.1 | – | – | – |
| Standard error | 3.8 | – | 2.1 | – | – | – |
| Standard deviation | 27.1 | – | 3.6 | – | – | – |

was able to be measured for 43% (n = 23) of the individuals in the whole sample, and ranges from 68 mm (the holotype) to 456 mm (MNHN.F.A50402, Jattiot et al. 2015: fig. 4.3).

*Gladius size and shape*: All the measured individuals have a triangular-shaped median field (Figs. 2 and 4A–C) with the widest section located at the anterior-most margin of the gladius. The shape of the anterior margin is slightly convex. This varies from the current diagnosis (Fuchs 2020), though it supports a previous, tentative interpretation (Fuchs 2006a: fig. 4). An anteriorly rounded imprint or contour on the ventro-medial section of the gladius is observed in four individuals (e.g., Fig. 4D). It is located just posterior to the anterior margin and bears a resemblance to the medial component of the head retractors seen in *Vampyroteuthis infernalis* Chun, 1903 (Bizikov and Toll 2016: fig. 12). As such, we suggest this feature corresponds with an attachment site for muscle tissue.

87% of the individuals have the slender (gladius width$_{max}$ to gladius length) gladius proportions of *Dorateuthis* (Table 3, SOM: table 3), though 13% show a very slender

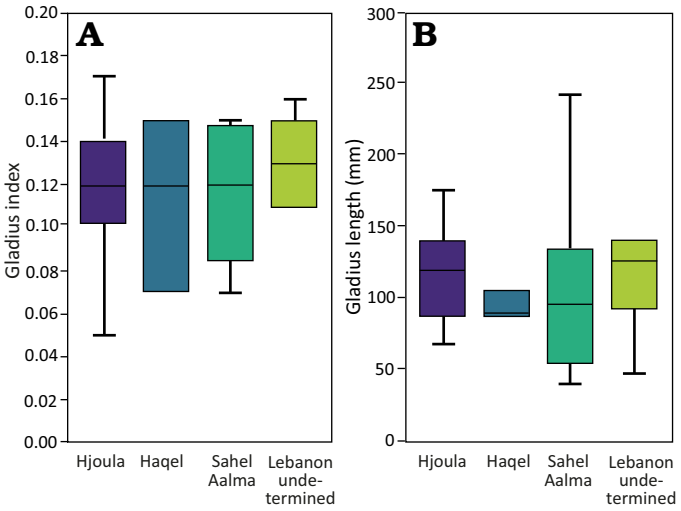


Fig. 5. Comparison of size ranges among the different sites sites in Lebanon using a gladius index (**A**) and gladius length (**B**). The gladius index is based on the ratio between gladius length and median field width. n = 8 (15%) of the sample were noted to be from the Santonian-aged site of Sahel Aalma, and the older Cenomanian localities of Haqel (n = 3, ~6%), and Hjoula (n = 36, ~67%). As a small number of the individuals from these Lebanese outcrops lack their specific locality information (n = 7, ~13%), a more general grouping of "Lebanon" was also included.

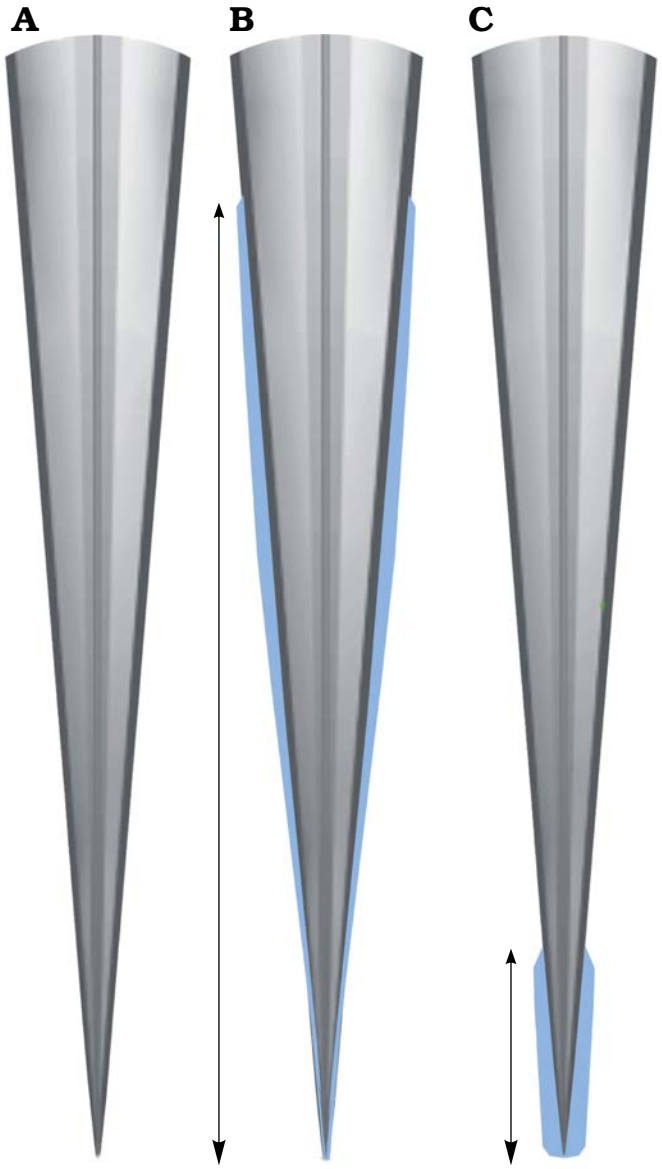


Fig. 6. The morphological variation observed in the lateral fields (in blue) of plesioteuthid coleoid *Dorateuthis syriaca* Woodward, 1883: not visible (**A**), anteriorly positioned (**B**), and posteriorly positioned (**C**). Modified from Fuchs (2006b, 2020). Not to scale.

gladius. All the individuals exhibit the requisite apical (opening) angle (<12°, mean of 6.9°). We found no statistical differences between gladius size, shape, apical angle, or body size, and any of the three specific localities (Fig. 5). However, Sahel Aalma shows the most size disparity as the smallest (the holotype, with a mantle size of 40 mm) and largest (MNHN.F.A50402, 241 mm) individuals are from this outcrop, which was not expected given the small sample size.

*Gladius reinforcements, lateral fields, and median field area*: Each of the 54 studied individuals has characteristic lateral reinforcements (keels) that are pronounced, and continuous from the anterior to the posterior margins of the gladius (Figs. 2, 4A–C). More than half of the sample (63%) exhibited some form of median reinforcements (Fig. 4A–C, SOM: table 4), longitudinally bisecting the gladius. These

median reinforcements vary and take the form of either a central medial line (Figs. 2, 4B) or ridge (Figs. 2, 4C), which may be uni- or bi-partite. A central median field, an elongate area in the central section of the median field (Figs. 2, 4A) may also be visible and span the line or ridge; they are also observed without a line or ridge. So far, there is no evidence to explain the type of median reinforcement exhibited. Longitudinal striations on the gladius (Fig. 4A, B) were commonly observed in the central median field in both dorsal and ventral view. These have previously been illustrated in plesioteuthids, such as *Plesioteuthis prisca* (Rüppell, 1829) (Naef 1922: fig. 42b) and noted to be "fine longitudinal lines" (translated from German).

The gladius has three observed morphological variations (Fig. 6). The most common type of gladius (78% of the sample) shows a complete absence of lateral fields (Fig. 6A). Seven individuals have anteriorly projected lateral fields (Fig. 6B), which extend approximately 80% to 90% along the length of the gladius. Four have elongated posterior lateral fields (30% of the gladius length) with no evidence of anterior lateral fields (Fig. 6C). These gladius morphotypes could not be associated with other soft tissue characters (e.g., arm length, total body size, or locality) in the study sample. It is possible that the variation observed is due to post mortem processes (e.g., mineral replacement across the gladii, disarticulation, or non-uniform compression), ontogenetic stage, dimorphism, or polymorphism enabling potential variation in muscular attachment (e.g., Toll 1998; Fuchs et al. 2016a; Bizikov and Toll 2016).

Where lateral fields were observed, the area of the median field was calculated following the formula given in Fuchs (2020) (median field area to gladius $area_{total)}$, who notes this is "very large" (>0.8) in *Dorateuthis*. All the individuals measured had a median field area >0.8 consistent with the diagnosis (SOM: table 3).

*Conus*: The conus is preserved in only two individuals, one in ventral view (Fig. 4E), the other in lateral. The length represents 3–5% of the gladius (conus $length_{max}$ to gladius $length_{max}$), and 80% of the width (conus $width_{max}$ to gladius $width_{max}$). No diagnostic indices currently exist for this character.

*Arms*: Twenty-two individuals (41%) provided the basis for arm measurements in this sample. Each of these individuals preserve at least one arm; nineteen preserve two or more, and only two show a complete arm crown. Both the latter individuals show the diagnostic differentiation in arm length noted for the species: a more elongated dorsal arm pair, a relatively short ventral pair, and two intermediate-sized pairs in lateral position (Fuchs and Larson 2011a: fig. 3). The three smallest individuals (gladius <50 mm) in the sample, including the holotype, show very little variation in arm length (SOM: table 2).

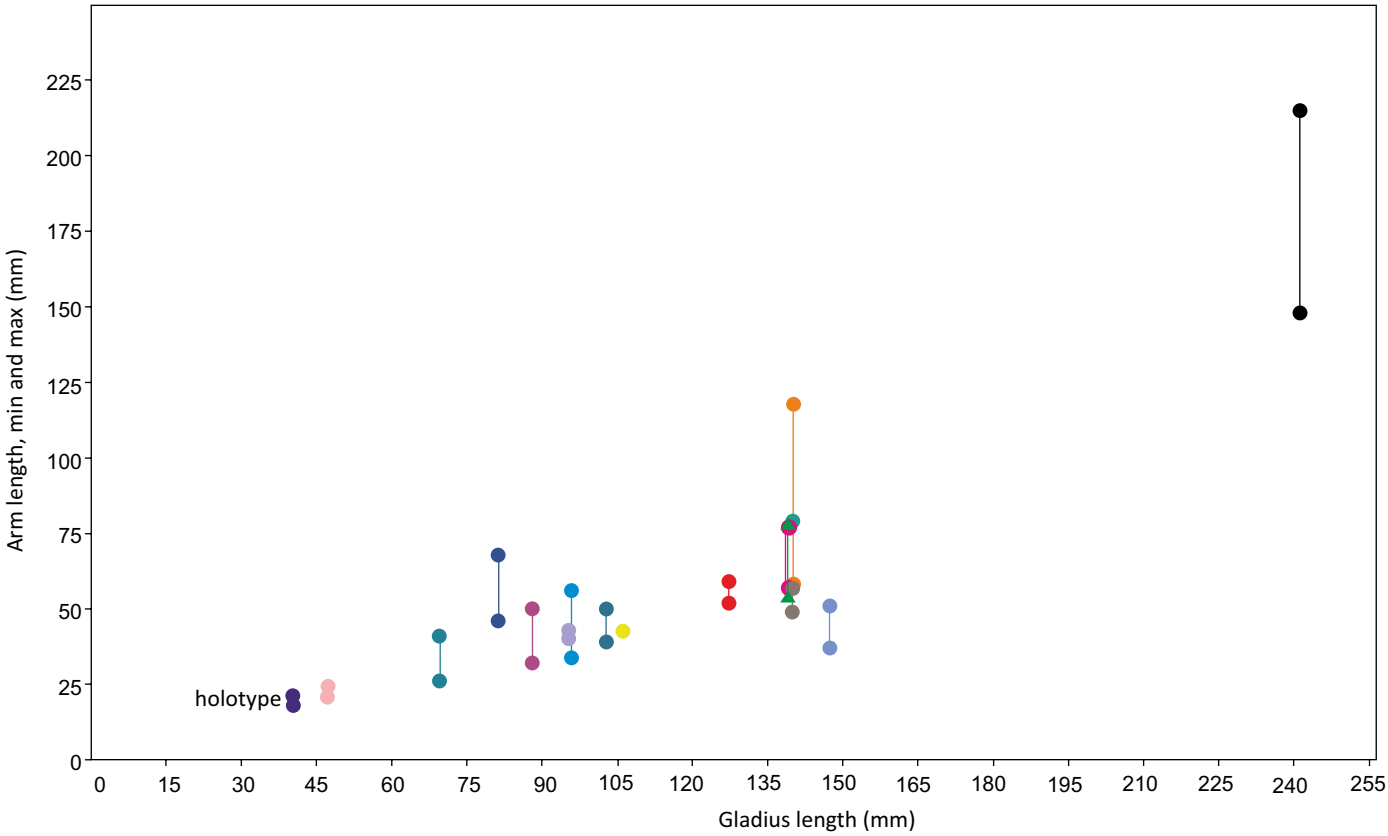


Fig. 7. Arm length vs. gladius median field length for the seventeen individuals that preserve at least two measurable arms, so that maximum and minimum values could be obtained. These upper and lower values are represented by two longitudinally paired points; the colour of each pair marks one individual. The results here support a relative increase in arm length with mantle length, as well as increased differentiation in the arm crown with mantle length.

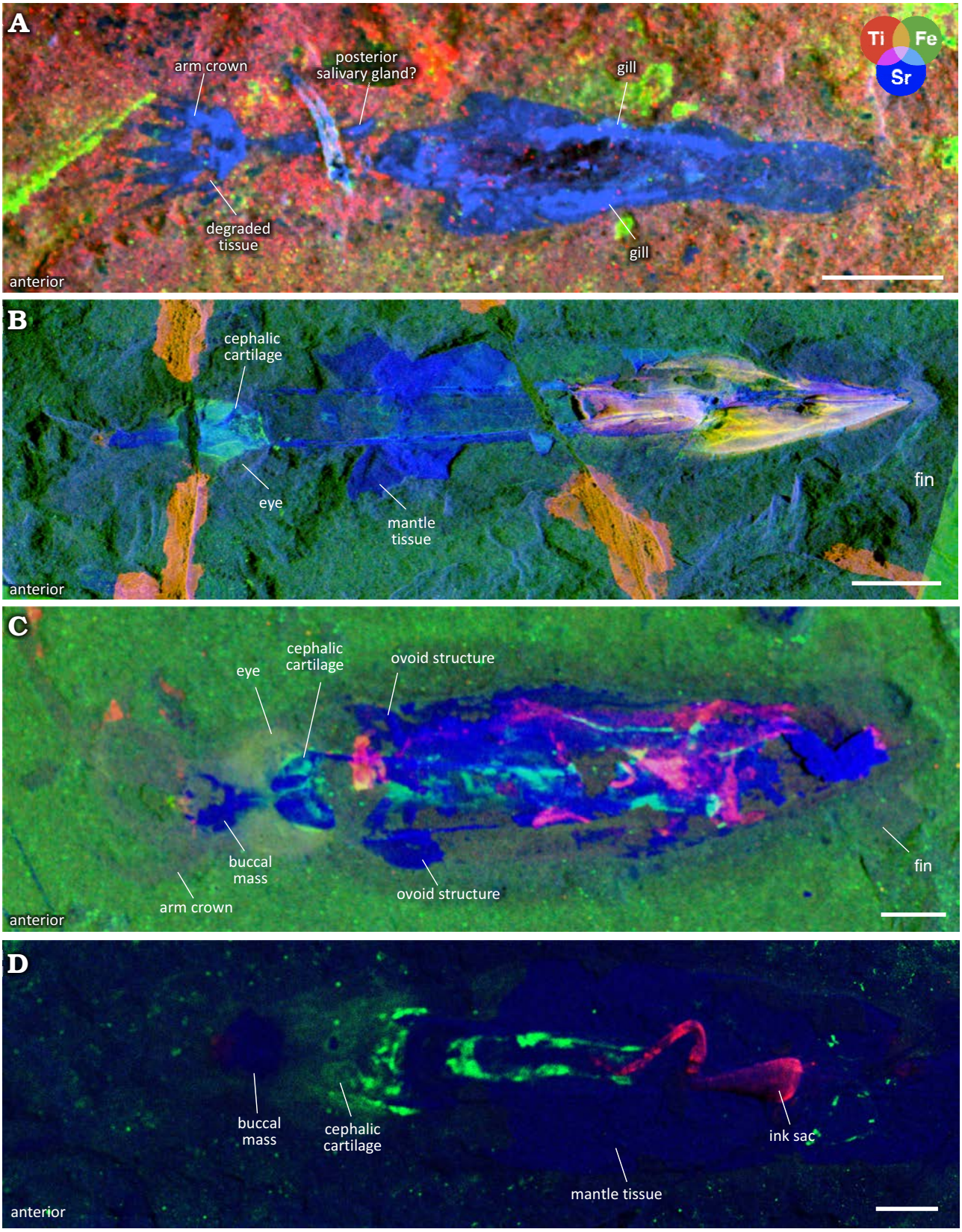


Fig. 8. µXRF major-to-trace elemental mapping of 4 individuals of plesioteuthid coleoid *Dorateuthis syriaca* Woodward, 1883, from Lebanon, with overlays of titanium (red), iron (green), and strontium (blue) distributions. Mantle tissue is commonly enriched in yttrium and strontium. This figure shows examples of strontium enrichment though yttrium exhibits the same distribution. **A**. BMNH C5017, holotype (Sahel Aalma, Santonian). **B**. MNHN.F.A88588 (Hjoula, Cenomanian). **C**. MNHN.F.A88589 (Hjoula, Cenomanian). **D**. BHI 2205 (Hjoula, Cenomanian). A, C, collected using the M6 Jetstream Bruker XRF, UAR 3224 CRC, MNHN; B, using the PUMA beamline, SOLEIL synchrotron; D, using Atlas X microXRF, iXRF Systems, Austin, TX. Scale bars 10 mm.

Comparisons between arm and gladius lengths were conducted (Fig. 7). These results indicated a general relative increase in relative arm length to mantle length as would be expected, supporting previous analyses that linked differentiation in the arm crown with allometry (Fuchs 2006a; Fuchs and Larson 2011a; Jattiot et al. 2015).

Chemical investigation reveals that the muscular mantle tissue of *D. syriaca* is commonly enriched in yttrium and strontium (Fig. 8) the presence of which is indicative of substitution for calcium in calcium phosphate (apatite) during diagenesis (Gueriau et al. 2018). This is consistent with phosphatization, a mode of preservation common in Cretaceous Lebanese coleoid fossil soft tissues (Clements et al. 2017; Klug et al. 2021c). Donovan and Fuchs (2016) supposed that arms were also preserved in apatite though they lacked mineralogical analyses. XRF data shows an enrichment in yttrium and strontium and supports their initial assumption (Fig. 8A). The substitution of these elements in varying soft tissues within a specimen has not been fully investigated, and this variation could be a diagenetic artifact, or could possibly reflect a bias

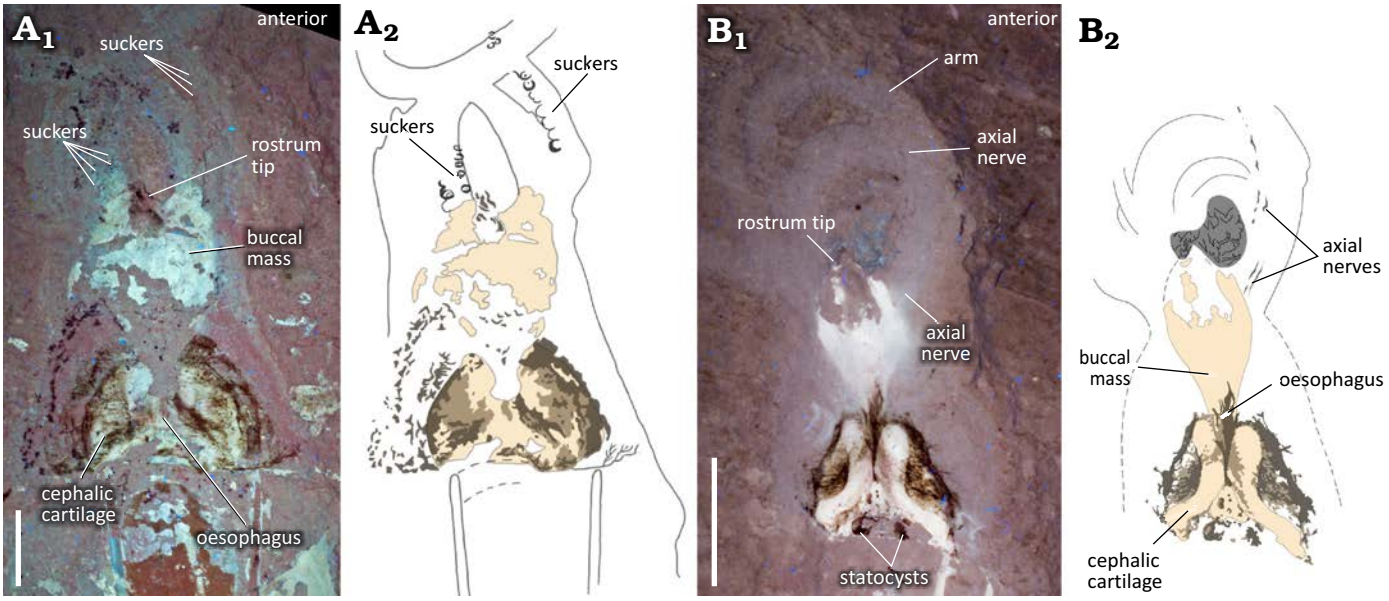


Fig. 9. Photographs ($A_1$, $B_1$, UV light), and interpretative line drawings ($A_2$, $B_2$) of the head and arm crown region of plesioteuthid coleoid *Dorateuthis syriaca* Woodward, 1883, from the Cenomanian of Houla, Lebanon. **A**. BHI 2229, in ventral ($A_1$), and dorsal ($A_2$) views. **B**. BHI 5779, in ventral ($B_1$) and dorsal ($B_2$) views. Though not well preserved, what we interpret to be suckers and axial nerves are identifiable. See SOM: fig. 3 for additional images of suckers. Illustrations by Jessica Gardner. Scale bars 10 mm.

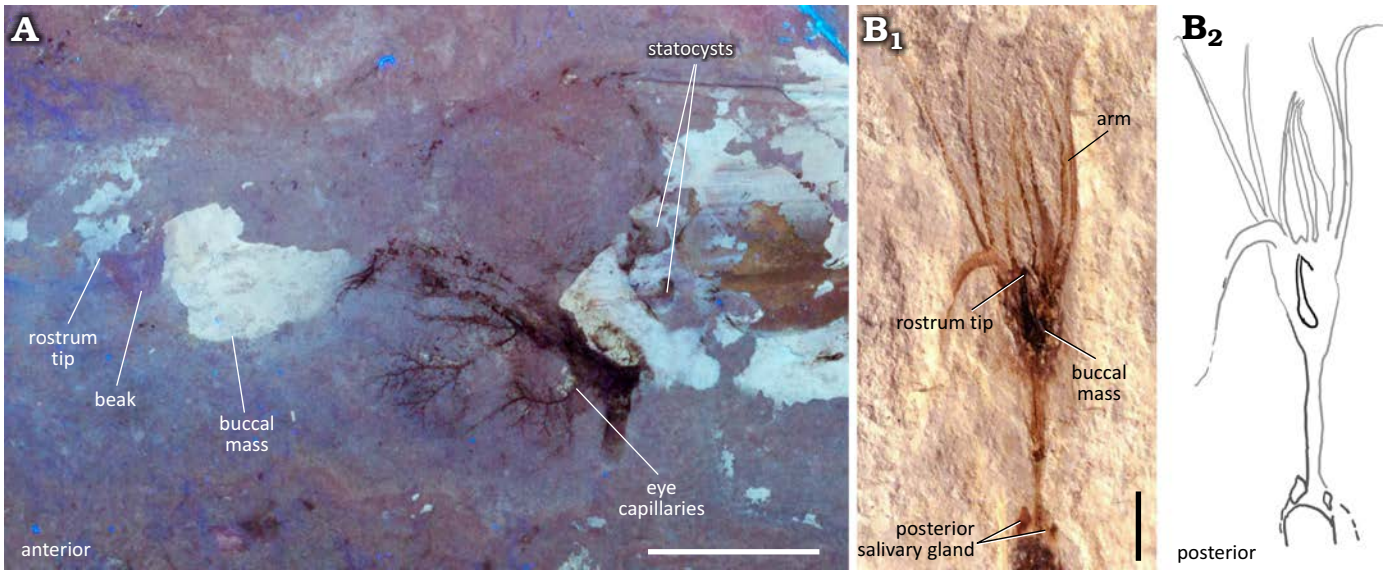


Fig. 10. Photographs (UV, natural light), and interpretative line drawing of the head and arm crown region of plesioteuthid coleoid *Dorateuthis syriaca* Woodward, 1883, from Lebanon. **A**. BHI 2203 (Hjoula, Cenomanian), dorso-lateral view preserving eye capillaries, beak, and statocyst. **B**. NHMW1998z0105/0000 (Sahel Aalma, Santonian), retaining the entire arm crown and posterior salivary glands; $B_2$ modified from Lukeneder and Harzhauser 2004: pl. 1.1. Scale bars 10 mm.

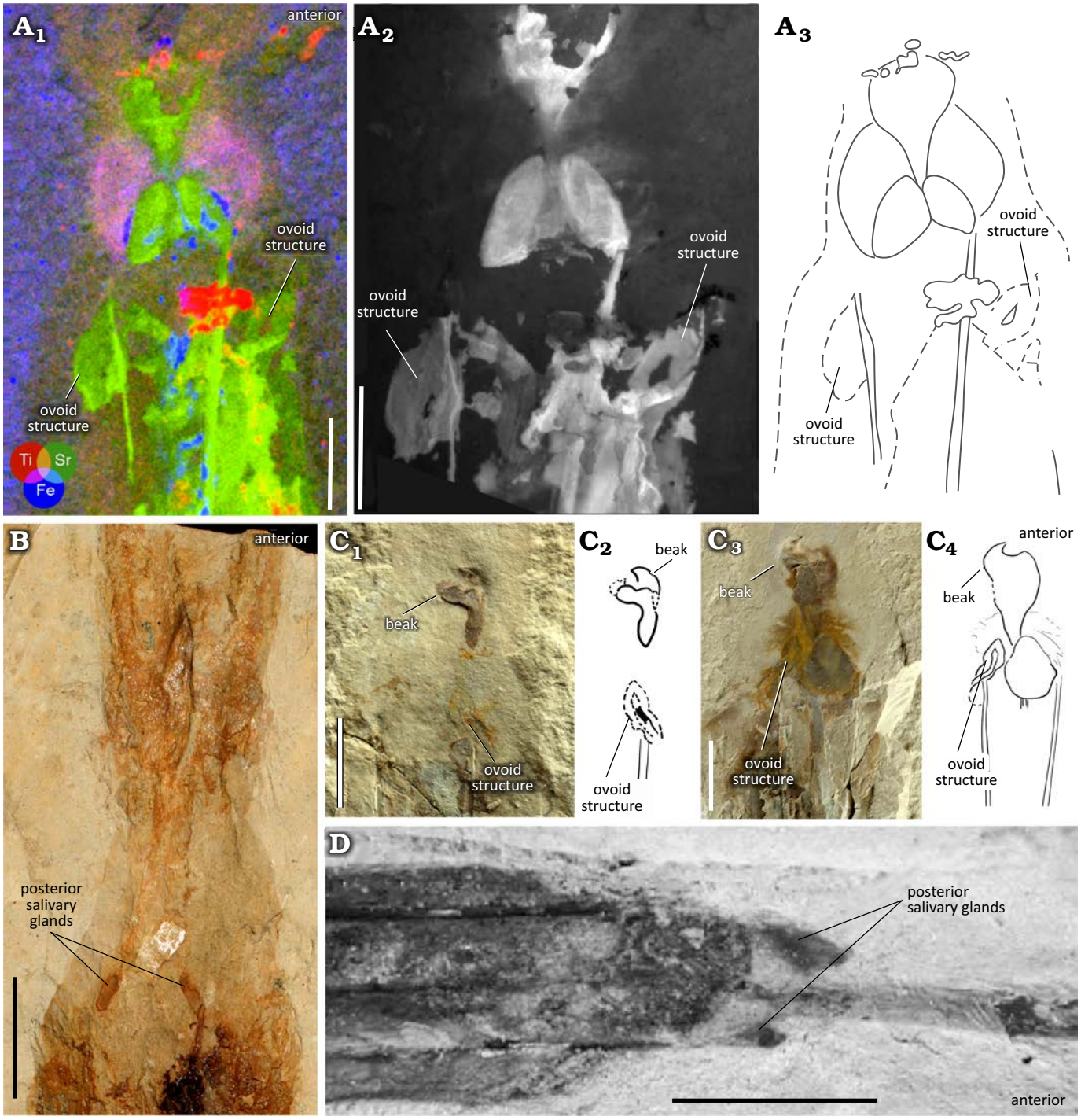


Fig. 11. Variation in paired structures associated with the anterior part of the gladius of plesioteuthid coleoid *Dorateuthis syriaca* Woodward, 1883, from Lebanon. **A**. MNHN.F.A88589 (Hjoula, Cenomanian): $A_1$, μXRF overlay of titanium (red), strontium (green) and iron (blue) distributions; $A_2$, luminescence emission at 385 nm under 514 nm illumination, UV-visible-near infrared multispectral imaging; $A_3$, interpretative line drawing. **B**. MNHN.F.50396 (Sahel Aalma, Santonian), image from the Reflectance Transformation Imaging (RTI) stack. **C**. NPL 52121 (Haqel, Cenomanian), $C_1$, part; $C_3$, counterpart; illustrations ($C_2$, $C_4$) and photographs ($C_1$, $C_3$) in natural light showing the ovoid structure and beak. **D**. NHMW1998z0105/0000 (Sahel Aalma, Santonian), from Jattiot et al. 2015: fig. 12.3. Note the two, pointed ovoid structures in A, and one pointed ovoid structure in C that are positioned adjacent to the external margins of the lateral keels. They appear different from the posterior salivary glands in MNHN.F.50396 (B) and NHMW1998z0105/0000 (D). Scale bars 10 mm.

of phosphatization, which is known to be highly selective of particular tissues (as outlined in Clements et al. 2022).

*Armature*: Eight individuals (15%) exhibit faint circular structures (~1–2 mm in diameter) on the arms that are interpreted here as suckers (Fig. 9A, SOM: fig. 1). These appear uniserial and radially symmetrical when observed under UV light. Although no individual has an entire row observable, we infer they were present along the entire length since

they are visible on proximal, medial, and distal portions of the arms in the separate specimens. There is no indication of attachment types, and no evidence of sucker linings, hooks, or cirri. Three individuals show remnants of the axial nervous system in the arm crown (Fig. 9B). These axial nerve elements (Klug et al. 2023; Rowe et al. 2023) are visible in UV light, and observed as delicate paired filaments, or dotted lines that follow the contours of the arms. Though one of these individuals have preserved the structure along the entire length of the arm, remnants are observed both proximally and medially (Fig. 9A, SOM: fig. 1).

*Head*: The cephalic cartilage (Fig. 9) is evident in 31% of the individuals. Using the methodology for determining orientation of the cephalic cartilage as outlined by Fuchs and Larson (2011a), we determine that in our samples it is preserved both dorsoventrally and laterally. It is most clearly visible in the UV photographs and elemental maps where the phosphatized cartilage fluoresces (Fig. $9A_1$, $B_1$). Structures interpreted as statocysts (e.g., Figs. 9B, 10A) are present on 4 individuals, just posterior to the cephalic cartilage. Internal calcareous statoliths (Boyle and Rodhouse 2008) are not observable.

Eye measurements were obtained on 15 specimens (28% of the total individuals). As we had more precise measurements for the gladius, the gladius length was used to identify a ratio for maximum eye diameter (gladius length:eye diameter 0.13–0.25) rather than follow the index of Young and Vecchione (1996), which compares the eye radius to head width. Five individuals also preserve evidence of a central eye lens, which can be observed in Fig. 10A by the positioning of the capillary system in the eye (Donovan and Fuchs 2016; Fuchs et al. 2016b; Fuchs and Larson 2011a). This appears in natural light as delicate filaments of yellow staining in a reticulated pattern. This pattern appears dark under UV light (Fig. 10A).

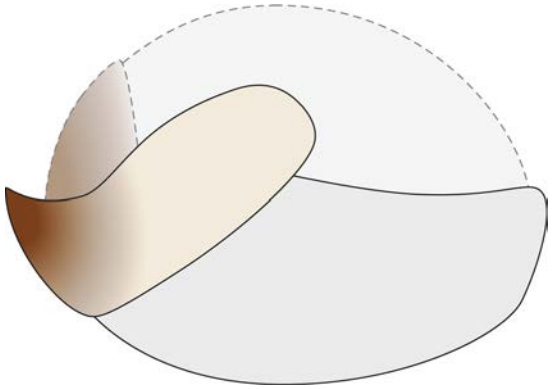

Fig. 12. Hypothesized beak reconstruction for plesioteuthid coleoid *Dorateuthis syriaca* Woodward, 1883, based on measurements from BHI 2203 (Hjoula, Cenomanian) and NPL52121 (Haqel, Cenomanian); see also Fig. 11C. Illustration by Alexandre Lethiers, CR2P. Not to scale.

Preservation of the buccal area is common and observed in ~72% of the individuals. The rostral tips, darker in colour than the rest of the beak chitin, are often visible under natural light. The muscular tissues of the buccal mass fluoresce under UV light (Figs. $9B_1$, 10A, $11A_3$). µXRF analysis demonstrates that the muscular tissue has elevated strontium traces compared with the matrix, indicating replacement of the original organic material by calcium phosphate (Gueriau et al. 2018). The length of the buccal mass was measured in 31 individuals. The ratio of buccal mass length/gladius

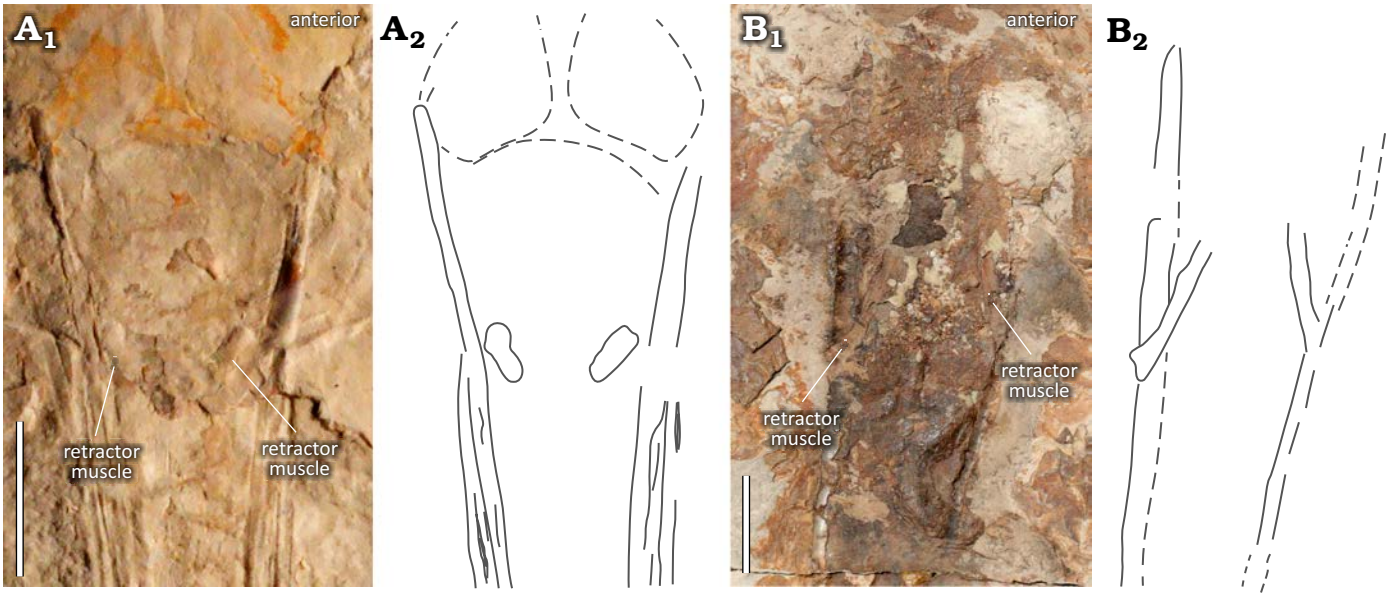


Fig. 13. Variation in paired structures interpreted as funnel retractor muscles or their insertions associated with the anterior part of the gladius of plesioteuthid coleoid *Dorateuthis syriaca* Woodward, 1883, from the Upper Cretaceous of Lebanon. **A**. BHI 2222 (Hjoula, Cenomanian), photograph in natural light ($A_1$) and interpretative drawing ($A_2$). **B**. MNHN.F.A50400 (Sahel Aalma, Santonian), RTI stack ($B_1$) and interpretative drawing ($B_2$). Both individuals have rope-like structures positioned posterior to the gladius anterior margin, which appear different from the paired structures shown in Fig. 11. Scale bars 10 mm.

length ranges from 0.08–0.19. More detailed measurements of the buccal mass were taken on individuals NPL52121 (Fig. 11C) and BHI 2203 to capture the 2D shape, which were scaled to provide a reconstruction, the first of its kind for *D. syriaca* (see Fig. 12).

*Posterior salivary glands and other paired structures*: Previous descriptive works on *D. syriaca* have identified a pair of posterior salivary glands located next to the anterior-most parts of the lateral margins of the gladius (Lukeneder and Harzhauser 2004: pl. 2.2; Jattiot et al. 2015: figs. 12.1, 12.2). Our study includes two individuals figured in Jattiot et al. (2015) and Lukeneder and Harzhauser (2004) (Fig. 11B and D respectively), that provide a comparator for this feature. The paired structures observed in the holotype closely resemble these posterior salivary glands.

Four individuals show paired structures that differ visually from the previously described posterior salivary glands (Figs. 11A, C, 13). Two exhibit ovoid-shaped imprints in the region of the anterior lateral keels (Fig. 11A, C). In natural light, one of these structures is visible laterally to the anterior gladius margin in both individuals (shown here in NPL 52121, Fig. 11C). The XRF and MSI images reveal a corresponding ovoid area, which is visible on the opposing side of the gladius margin. But for the shape, there is no evidence to suggest that this is anything other than mantle tissue. As such, it is possible that this ovoid structure reflects the anterior section of a funnel. The other two individuals possess paired structures with a rope-like morphology (Fig. 13). These are either visible as hemispherical projections anteriorly angled towards the lateral keels (Fig. 13A), or medially angled inwards from the lateral keels (Fig. 13B) and are interpreted here as remnants of funnel retractor muscles (Bizikov and Toll 2016; Fuchs et al. 2016a).

*Digestive system*: Preserved digestive contents are present in 19 individuals. Typically, the remains are ingested, and their relative position in the body enables comparison with the digestive organs in extant coleoids (Mangold and Young 1998; Wells 2011). One individual (MNHN.F.A88589) preserves remains in 3 areas (Fig. 14$A_1$–$A_4$): two are positioned in the posterior section of the mantle (Fig. 14$A_1$, $A_3$, $A_4$) and likely reflect the stomach and caecum. The composition of these remains varies which supports the different functions of these two digestive organs. The mass of digestive remains interpreted here to be stomach contents (Fig. 14$A_3$), contains an articulated ray fin and a pelvic girdle, likely from a teleost fish; the posterior-most mass (Fig. 14$A_4$) has a collection of less distinct, individual bones surrounded by a soft mass and likely represents caecal contents. The third mass of digestive remains (Fig. 14$A_2$) is positioned more anteriorly in the mantle, is tubular in shape, and also retains evidence of fish bones. The position and contents are consistent with the presence of a crop.

The individuals examined in the study enabled observation of almost all elements of the digestive system of *D. syriaca*. While the preservation of ingested food matter is not uncommon in organisms that are phosphatically preserved

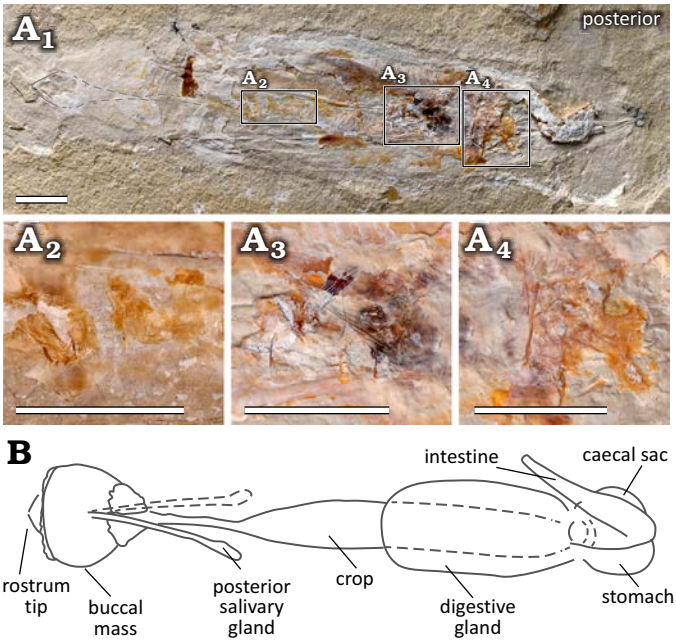


Fig. 14. Components of the digestive system of plesioteuthid coleoid *Dorateuthis syriaca* Woodward, 1883, from the Cenomanian of Houla, Lebanon. **A**. Individual MNHN.F.A88589 in natural light ($A_1$), showing three separate areas preserving digestive contents, which indicates the presence of a crop, stomach, and caecum; $A_2$–$A_4$, close ups of the digestive contents from individual images of the RTI stack. Scale bars 10 mm. **B**. An illustration of the vampyromorph digestive system modified from Mangold and Young (1998) and provided here for reference. The vampyromorph, *Vampyroteuthis infernalis* Chun, 1903, is described with one posterior salivary gland, here, we observe two for plesioteuthid coleoid *Dorateuthis syriaca* Woodward, 1883 (Fig. 11B, D). Photograph in natural light ($A_1$) by Lilian Cazes, MNHN. Not to scale.

(see Clements et al. 2022), phosphatization appears to be highly selective in terms of which tissues are replaced by apatite—and while ingested organics appear to preferentially phosphatise, internal digestive integument is comparatively rare in the fossil record (Clements et al. 2022). This seems to be the case in *D. syriaca,* however, the relative positions of the ingested organics within the organism allows the determination of an Octobrachia-like gut configuration. One key character identified by this study is the crop of *D. syriaca*; the presence of a crop is known in Recent Vampyromorpha (Fig. 14$A_5$) and most Octopoda, but it is absent in modern Decabrachia (Mangold and Young 1998: fig. 1). As such, this configuration of the digestive system is consistent with the assignment of *Dorateuthis* to Octobrachia.

*Funnel*: A funnel can be inferred in BHI 2213, preserved in dorso-lateral view (Fig. 15B). The feature was not observed directly, though its presence was determined by a stained elongated mass within the boundaries of the mantle. The staining is interpreted here to delineate the internal part of the funnel. The anterior margin of this is located just posteriorly and ventrally to the head, consistent with the placement of the funnel in both fossil and modern coleoids.

This stained impression shows evidence of diagenetic circular structures (Fig. 15B) associated with the presence of

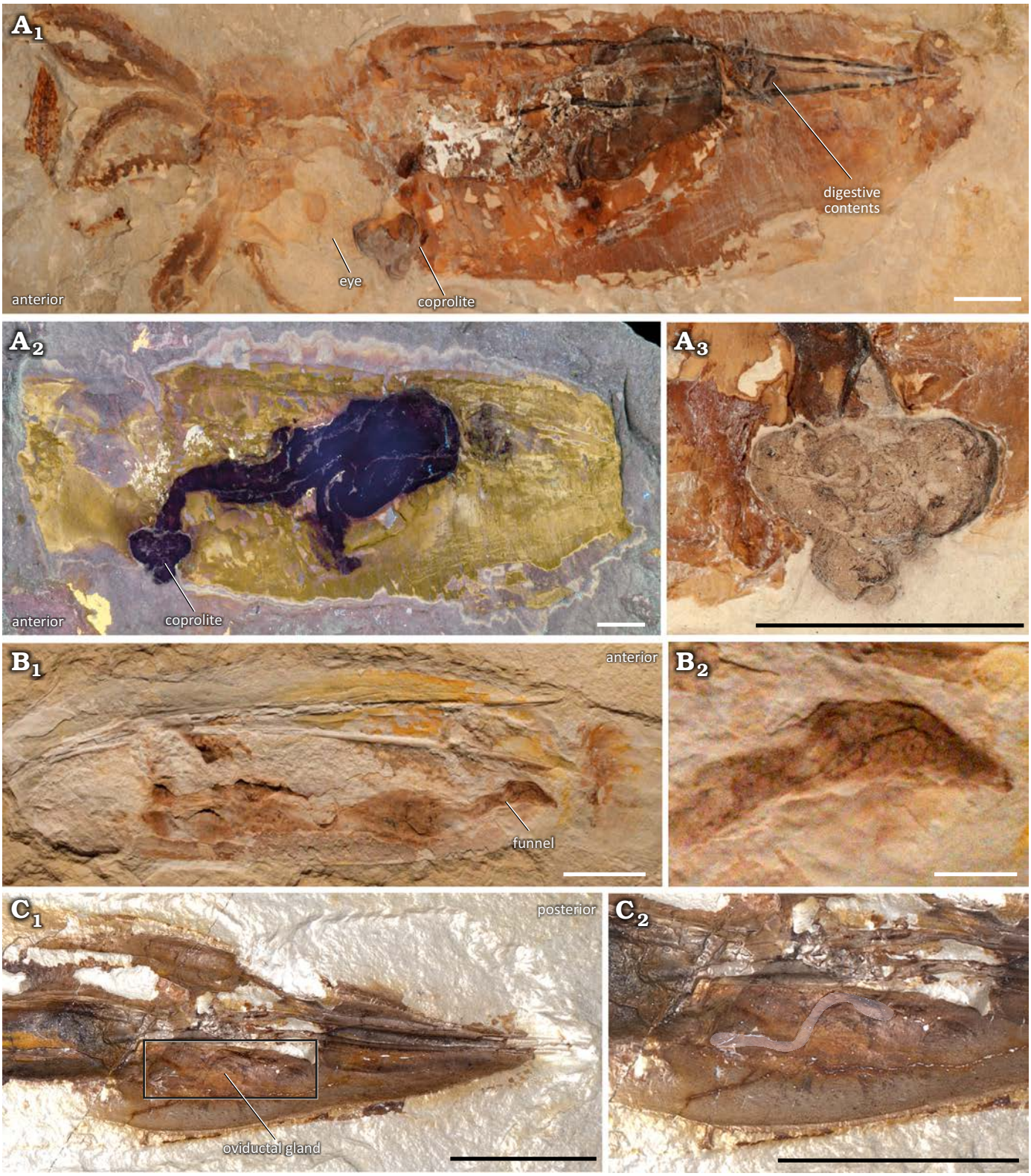


Fig. 15. Digestive and possible reproductive elements of plesioteuthid coleoid *Dorateuthis syriaca* Woodward, 1883, from the Upper Cretaceous of Lebanon. **A**. MNHN.F.R06746 (Sahel Aalma, Santonian) is dorso-laterally preserved, and the funnel is inferred; $A_1$, part, individual image from the RTI stack; $A_2$, counterpart under UV light; $A_3$, a coprolite preserved at the anterior aperture of the funnel. **B**. Photographs of BHI 2213 (Hjoula, Cenomanian) in natural light showing the entire mantle with the funnel in situ ($B_1$), and a close-up of the anterior-most part of the funnel ($B_2$). **C**. Individual image from the RTI stack of MNHN.F.A88589 (Hjoula, Cenomanian) in the Spectacular Enhancement rendering mode showing the region of a possible oviductal gland ($C_1$), and a close-up with overlay of the same ($C_2$). Photograph in $A_2$ by Lilian Cazes, MNHN. Scale bars 10 mm.

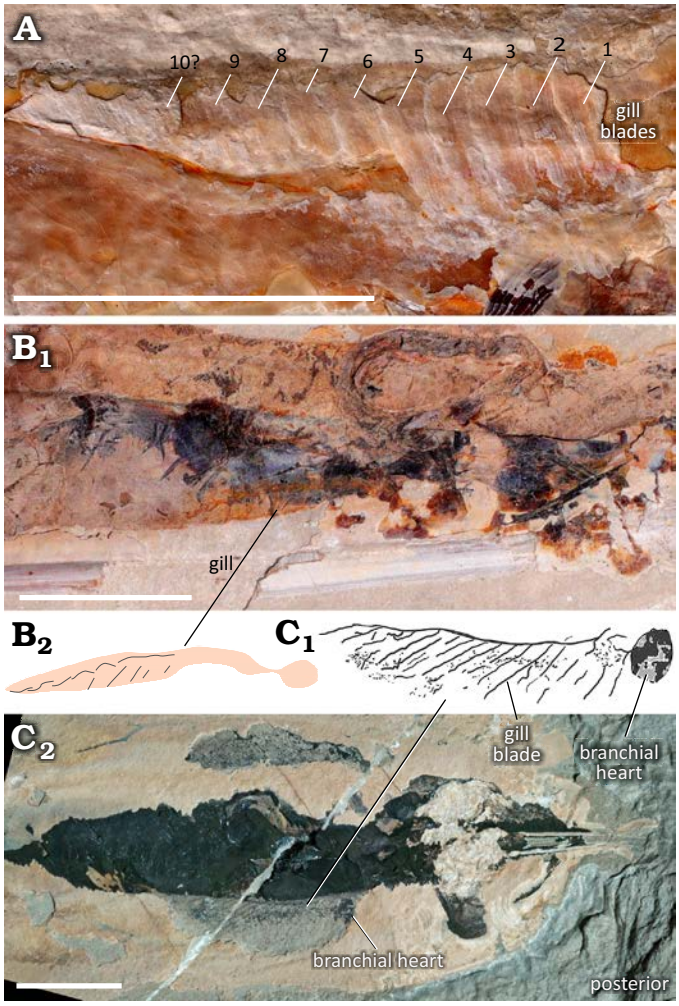


Fig. 16. Gill preservation in plesioteuthid coleoid *Dorateuthis syriaca* Woodward, 1883, from the Cenomanian of Houla, Lebanon. **A**. RTI image of MNHN.F.A88589 showing impressions of at least 10 gill blades **B**. RTI image of MNHN.F.A88590 ($B_1$) and simplified illustration ($B_2$), showing preservation as orange stains. **C**. BHI 2219, photographed in natural light ($C_1$). The gills appear black in colour, possibly a result of ink-staining. The branchial heart is observable in the posterior part of the gill structure (illustrated in $C_2$). Scale bars 10 mm.

ink (Klug et al. 2021c). These circular patterns are also present in individual MNHN.F.R06746 on an unresolved structure (Fig. 15$A_3$). Roger (1946) suggested it was a rectal bulb (translated from French), and Jattiot et al. (2015) indicated it may be a buccal mass. Given its location (Fig. 15A) and the presence of the diagenetic circular patterns, we interpret this structure to represent an accumulation of the long strings of pigmented faeces (coprolite) released from the mantle via the funnel (Boyle and Rodhouse 2008).

*Gills*: Remains of gills are present in 12 individuals (22%). They are preserved either as impressions (Fig. 16A), orange/yellow (Fig. 16B), or black stains (Fig. 16C). The orange staining of the gill relics represents pyritization, rather than phosphatization (Donovan and Fuchs 2016). The most complete gills (Fig. 16C) show the branchial heart (~2 mm length $_{max}$), the main efferent vessel (~14 mm), and a minimum of 17 gill blades. Combined, this represents ~21% of the gladius length. The associated lamellae are not preserved, though the filamentous gill blades taper distally (~4–1.3 mm). Lamellae (n = minimum of 9) and gill blades are present in MNHN.F.A88589 (Fig. 16A). Under natural light, the blades are visible as orange filaments, and the lamellae are preserved as contoured relief. No main efferent vessel is observed.

*Fins*: The "oar-shaped" fin described for *D. syriaca* (Fuchs 2020: fig. 3, 1e) is observed in the holotype from the Santonian of Sahel Aalma (Fig. 3$A_1$, $A_2$, B), as well as six (~11%) other individuals (Fig. 17) from the Cenomanian outcrops. It is preserved as a mineralized structure (Fig. 17A), an impression (Fig. 17B) or an orange-coloured stain (Fig. 17E), making it generally distinguishable from the matrix under natural light. Its visualization can be enhanced using μXFR elemental mapping (Figs. 8B, C and 17D) and/or UV photography (Fig. 17C, F).

*Reproductive system*: Reproductive organs were tentatively included in a summary of known soft tissues in *D. syriaca* (Donovan and Fuchs 2016). This was based on a description by Roger (1946: fig. 7) of spermatophores in individual MNHN.F.R06746. Observations on this individual show that what Roger (1946) interpreted to be spermatophores are, instead, digestive contents (Fig. 15$A_1$). However, in MNHN.F.A88588 there are impressions present which possibly represent oviductal glands (Fig. 15C). These correspond with a titanium-enriched area that is observable using μXRF mapping (Fig. 8B).

*Novel anatomic characters of* Dorateuthis syriaca: The multimodal imaging approach and quantitative analyses performed in this work has enabled a revision of the summary of known soft tissues in *D. syriaca* (Fig. 18, SOM: table 5) that were previously synthesized in Donovan and Fuchs (2016). Furthermore, we have identified morphological characters, which were not previously described for the genus including paired retractor muscles, axial nerves in the arms, and an Octobrachia-type digestive system. For the first time, we also provide clear evidence of a funnel, circulatory system, and excretory system. Lastly, we discount the presence of tentacles, tentacular pockets, and hooks within the arm crown, and confirm that *D. syriaca* possessed suckers.

*Stratigraphic and geographic range*.—Lower upper Cenomanian–upper Santonian of Lebanon.

# Discussion

**General taphonomy**.—Despite the exceptional preservation of coleoids from the Lebanese localities, it is vital to acknowledge that all fossils have undergone decay prior to fossilization, and therefore, do not represent an anatomically complete organism (e.g., Purnell et al. 2018; Clements et al. 2022). Additionally, the depositional environments and diagenetic processes of Lebanese Lagerstätten are currently poorly understood and no comprehensive taphonomic model for Lebanese coleoid fossils has yet been undertaken

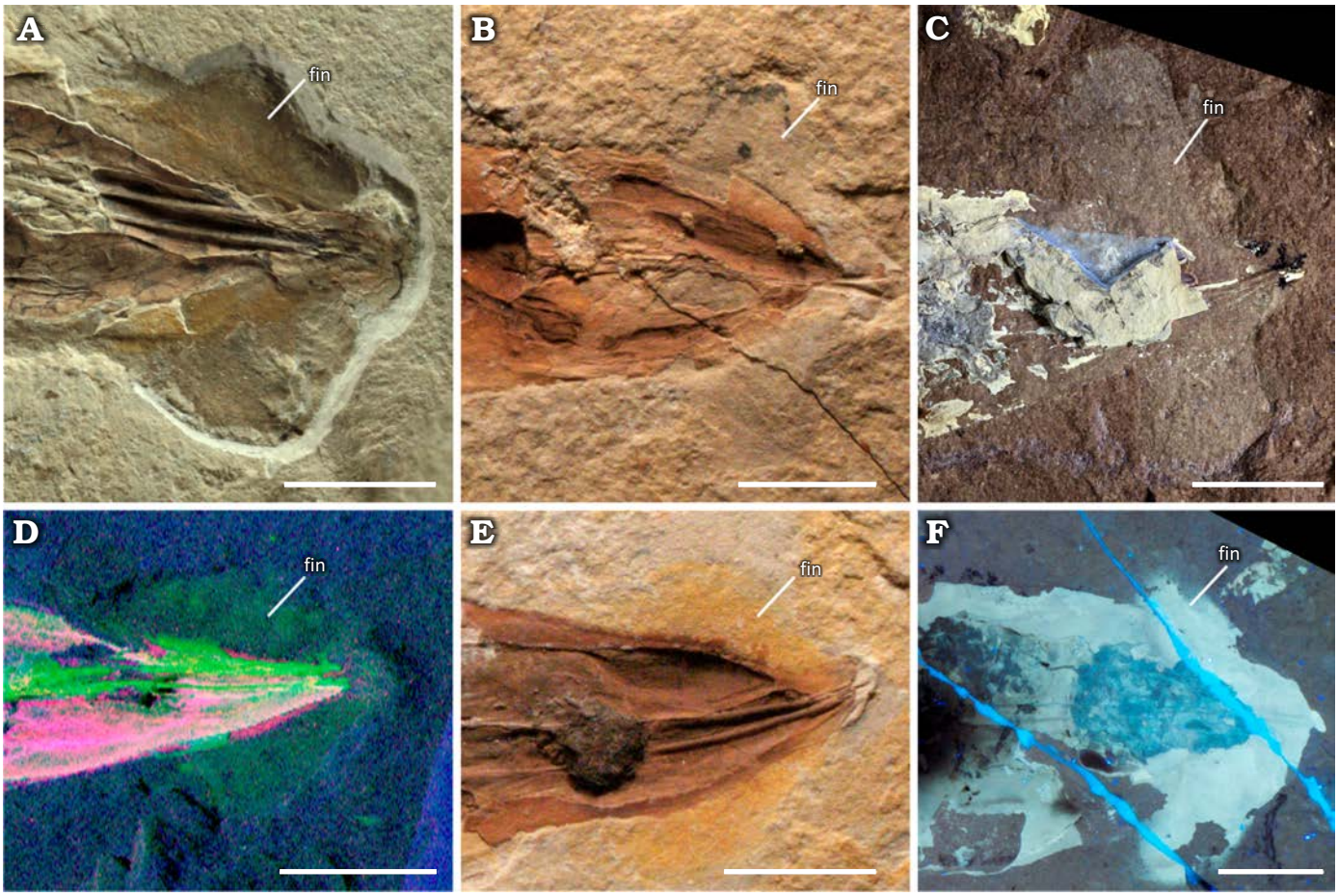


Fig. 17. "Oar-shaped" fins of plesioteuthid coleoid *Dorateuthis syriaca* Woodward, 1883, from the Cenomanian of Lebanon. **A**. NPL52121 (Haqel), natural light. **B**. BHI 2212 (Hjoula), natural light. **C**. MNHN.F.A88589 (Hjoula), UV photograph (Lilian Cazes, MNHN). **D**. MNHN.F.A88588 (Hjoula), µXRF overlay of titanium (red), strontium (green) and iron (blue) distributions. **E**. BHI 2227 (Hjoula), natural light. **F**. BHI 2205 (Hjoula), UV photograph provided by DF. Scale bars 10 mm.

(George et al. 2024). However, the most common mode of soft tissue preservation in these deposits is through phosphatization, a process of authigenic mineralisation (typically by calcium phosphate) that replaces the labile tissues with mineral replicas. As such, the morphology of the tissue is retained though the original organic tissues themselves are lost. This relatively rapid mode of preservation is dependent on specific environmental conditions which are reviewed in Clements et al. (2022). As shown here, the various tissues and organs of *Dorateuthis syriaca* are not all preserved to the same extent (see SOM: table 5). For example, the ink sac and parts of the muscular mantle are commonly preserved and seen in almost all the individuals in the study. The tissues from the arm crown and fins, however, are much less common. Some of the least represented elements are those of the reproductive system, and axial nerves of the arms.

**Morphological variation in the gladius**.—To further complicate our interpretation of the fossil material, there are many uncertainties regarding the existing diagnostic characters of *Dorateuthis* and more specifically *D. syriaca* (Woodward 1883; Roger 1946; Fuchs 2006a, 2007; Fuchs and Larson 2011a; Jattiot et al. 2015). For example, previous observations on the posterior lateral fields have been conflicting, and both elongate (Fuchs 2006a: pl. 1: B) and rounded lateral fields (Fuchs and Larson 2011a: fig. 2.7) have been described. As such, there is no definitive diagnosis on the lateral fields in *Dorateuthis* (Fuchs 2020). Our observations of the elongated posterior lateral fields are consistent with the interpretation of Fuchs (2006a).

In Mesozoic coleoids, the muscular mantle was attached to the lateral margins of the gladius with the lateral keels (reinforcements) providing strength to the median field (Fuchs et al. 2016a, b). The fins were inserted either into the hyperbolar zones or dorsal margin of the lateral fields (Fuchs et al. 2016a). For the first time, this study describes long anterior lateral fields in *D. syriaca*, which resemble those seen in *Plesioteuthis prisca* (Rüppell, 1829) from the Tithonian of Solnhofen and the contemporaneous *Boreopeltis smithi* Fuchs & Larson, 2011a (Fuchs 2020). It is possible that the extended lateral keels in *D. syriaca* added extra support and rigidity to the mantle and fins during locomotion. If this is the case, we could infer that both prototeuthids from Lebanon, *B. smithi* and *D. syriaca* benefited from increased levels of mantle stability and exploited active locomotion.

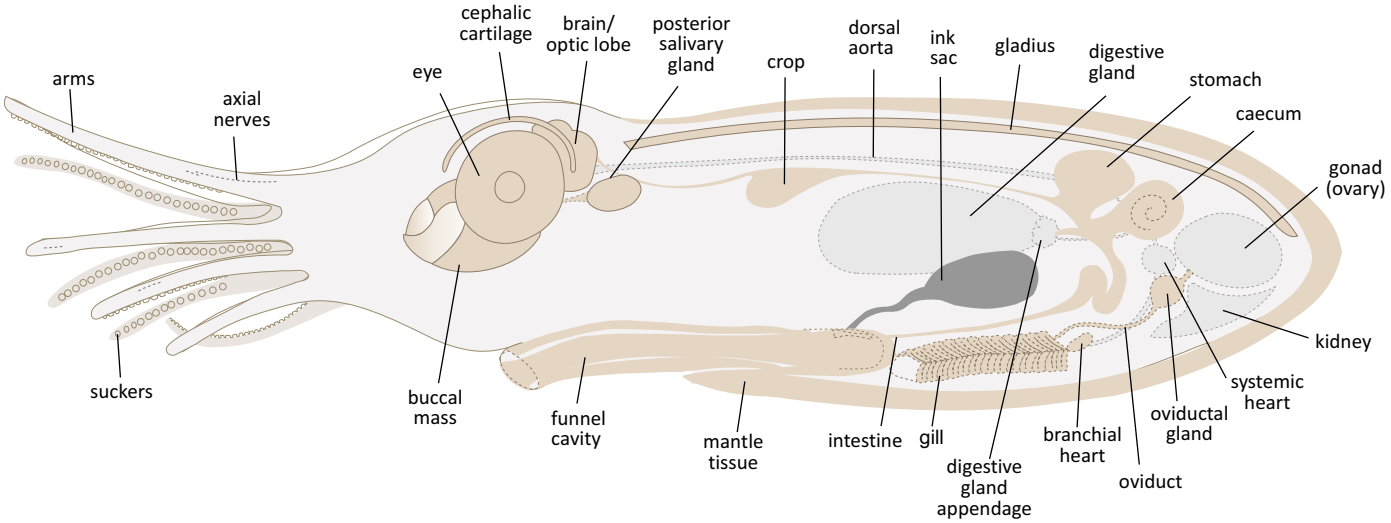


Fig. 18. A hypothesized illustration of the internal anatomy and arm elements of plesioteuthid coleoid *Dorateuthis syriaca* Woodward, 1883, based on both the anatomical observations in this study in combination with the anatomy of extant Octobrachia. Organs and tissues that were observed are represented in brown, while those that are part of extant forms but not observed here, are in pale grey (with the exception of the ink sac, which was the most commonly preserved organ in this study). The external proportions of the head and arm crown are based on the adult reproduction in Fig. 19 (this paper). The body profile has been extended dorso-ventrally to reduce the potential for overlapping organs and show the anatomy more clearly. Not to scale.

An analysis of other prototeuthid genera, and taxa contemporaneous to *Dorateuthis* (Fuchs 2020), shows no evidence that this variation can be attributed to mistaken identity (SOM: table 6). As such, the polymorphism observed—the variation in the presence and location of the lateral fields, as well as the differences in the median reinforcements—adds to the complexity of what is known about this structure in *D. syriaca.* There are no clear links to local effects or the time difference between localities (Fig. 5). We interpret the observed morphological variation to be associated with either dimorphism or ontogenetic stage, as these are known to contribute to interspecific variation in extant gladii (e.g., Toll 1998; Bizikov and Toll 2016).

**Size**.—The measurements obtained on the individuals in the sample enabled a hypothesized reconstruction for the holotype (likely a juvenile; see below), and an "average-sized" individual of *D. syriaca* (Fig. 19). The two reconstructions show a large variation between the smallest and largest individual. The smaller size is not interpreted to be related to sexual dimorphism as our analyses show no distinctions indicative of more than one grouping (SOM: figs. 2, 3). Additionally, there appears to be no size selectivity by locality (Fig. 5A). Overall, the size of *D. syriaca* seems to be conservative despite the ~10 Ma age difference between the Cenomanian and Santonian sites. Despite having only eight individuals (15% of the total studied sample) from Sahel Aalma, the locality shows the greatest size disparity as the smallest and largest outliers are from the site (SOM: fig. 5B). More individuals from museum collections, would need to be studied to determine if this is a real signal in Sahel Aalma, or if this reflects a sampling bias.

The body size (including head and arms) was determined for 23 individuals. Even in the best-preserved individuals, precise measurements are difficult to obtain as boundaries in the 2D phosphatized individuals are not always clear. However, the characteristic arm crown configuration for *D. syriaca*—an elongate dorsal pair, a shorter ventral pair, and two intermediately sized lateral pairs (Fuchs and Larson 2011a)—is clearly present. This pattern was not observed in the three smallest individuals (mantle size <50 mm). Instead, they showed minimal length variation in the arm crown giving the appearance of arms that are all similar in length.

Seventeen individuals preserve two or more arms. Plotting the maximum and minimum arm lengths from these individuals shows a correlative increase in arm length to mantle length (Fig. 7). This supports the hypothesis that the relative arm length is linked with the ontogenetic stage (Fuchs 2006a; Fuchs and Larson 2011a; Jattiot et al. 2015). Here, we suggest that the most likely explanation of the smaller sizes observed in the entire study sample (Table 4) is that it is comprised mostly of juveniles, and the genera-level description in Fuchs (2020) included more mature individuals. Additionally, we hypothesize that the three smallest individuals, with minimal differentiation in the arm crown, represent young juveniles.

**Systematic and phylogenetic implications**.—*Dorateuthis syriaca* is included in several published morphological matrices that contain both fossil and extant taxa. Initially published by Sutton et al. (2016), the matrix was minimally modified to assess the phylogenetic position of *Proteroctopus* Fischer & Riou, 1982 (Kruta et al. 2016) and *Vampyronassa* Fischer & Riou, 2002 (Rowe et al. 2022) and underwent a more extensive revision by Whalen and Landman (2022). Our study provides new character state information on 21 of the 153-character states for *D. syriaca*, 6 of which are specific to the gladius (SOM: table 7).

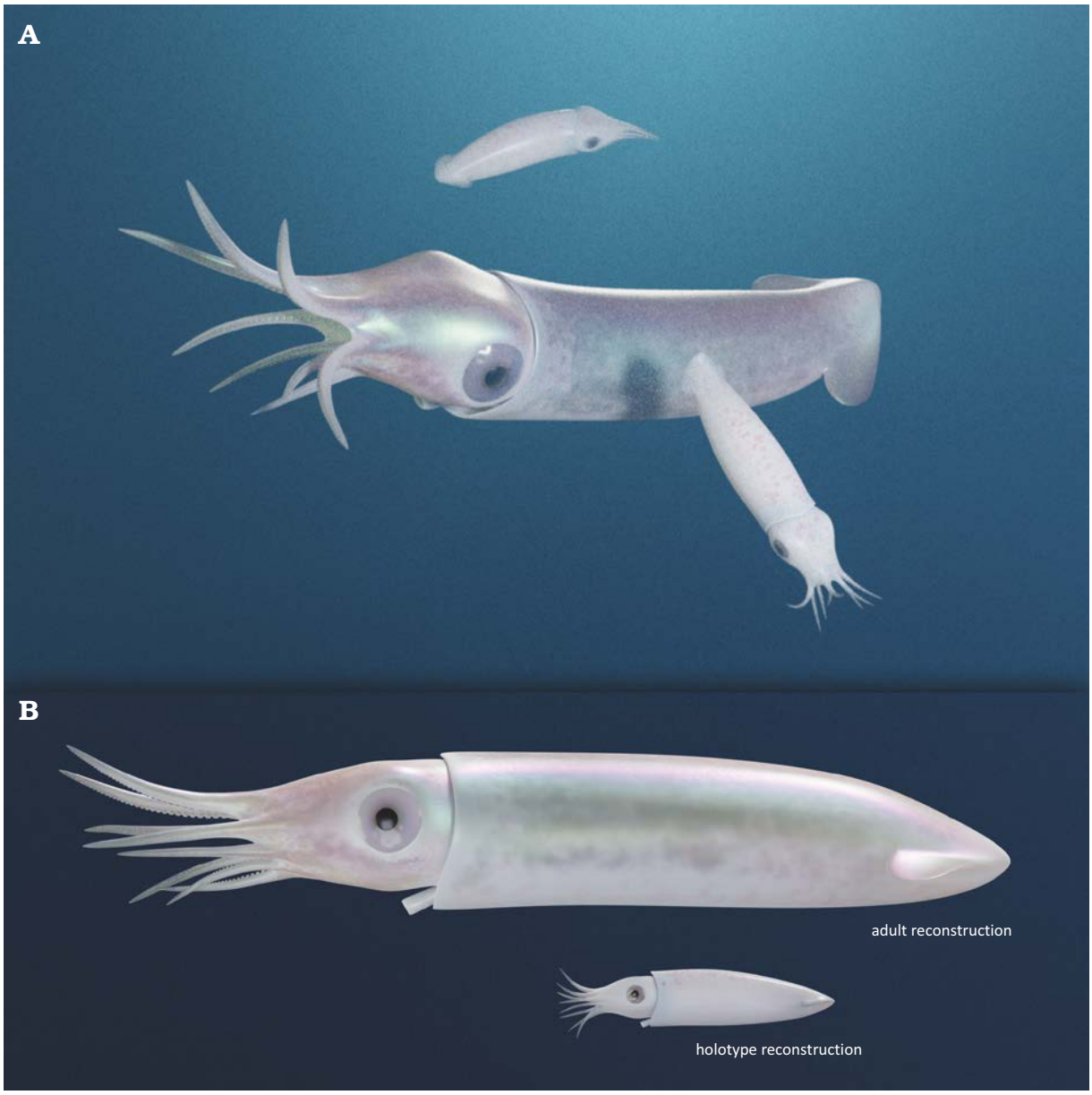


Fig. 19. Hypothesized reconstructions of plesioteuthid coleoid *Dorateuthis syriaca* Woodward, 1883, in inferred life positions (**A**), and lateral view (**B**). The larger individual in B reflects an average, medium-sized *D. syriaca*; the smaller is a reconstruction of the holotype, which is considered to be a juvenile. The reconstruction of the holotype was based on direct measurements of visible structures revealed by the μXRF, RTI, and UV imagery. As it was not possible to obtain measurements of all the preserved soft tissue on one individual, measurements from four individuals were used and scaled to the correct size. BHI 2232 (Hjoula, Cenomanian) provided the basis for the reconstruction. Scaled elements were obtained from BHI 2203 (eye and lens diameter), NHMW1998z01050000 (arm lengths), and BHI 2227 (fins). These are from Hjoula (Cenomanian), Sahel Aalma (Santonian), and Hjoula (Cenomanian), respectively. Reconstructions Alexander Lethiers, CR2P. The mantle length is approx. 139 mm in the adult and approx. 40 mm in the holotype.

Although the gladius of coleoids is a relatively simple structure, it contributes approximately half of the character states to the systematics of fossil and extant coleoids (Sutton et al. 2016; Whalen and Landman 2022). However, ambiguity regarding certain terminology introduces inherent issues, for example, when determining median reinforcements and fin shape. Currently, *D. syriaca* is coded as possessing a convex median keel (characters 54/55, Whalen and Landman 2022). However, this is in contrast with descriptions in the literature for both the genus and species, which specifically notes the absence of a keel (Fuchs and Larson 2011a: 238; Fuchs 2020: 10). Following these authors, the terms "line" or "ridge" were used here to reflect the level of robustness. Uncertainty around this definition can be seen in the original description of *D. syriaca*, in which Woodward (1883) uses both ridge and line seemingly interchangeably.

There is a similar vagueness around the classification of fin shapes; inconsistencies which have already been acknowledged (Sutton et al. 2016). The diagnostic shape for *Dorateuthis* is "oar-shaped" (Fuchs 2020), which is visually like the "rhomboid" shaped fin illustrated by Hanlon et al.

(2018). Citing this issue, Sutton et al. (2016) coded only for two shapes, lobate and rhomboidal. Currently, *Dorateuthis* is coded as lobate (Whalen and Landman 2022). Determining the states for fin shape will continue to be limiting without a more concise terminology (Young et al. 2001). As the current systematic framework for Mesozoic coleoids has many inherent, widely recognized uncertainties (e.g., Young and Vecchione 1996; Lindgren et al. 2004; Kruta et al. 2016; Sutton et al. 2016; Fuchs 2020; Whalen and Landman 2022), a phylogenetic analysis was not conducted here. However, this study has revealed previously unknown information on multiple characters and characters states that provides new data for future systematic analysis (SOM: table 7). This includes states that were previously coded as unknown (presence, placement and symmetry of suckers; absence of arm pair II; shape of the eyes; presence of the outer capsule of the statocyst; presence and placement of the posterior salivary gland, and a bipartite ventral interruption), as well as states that need to be amended (the polymorphic states of the lateral fields; shape of the anterior gladius margin and tip; absence of a keel and presence of lines and ridges; presence of thin lateral plates on the dorsal median field, and the absence of cirri on the arms).

In the most recent morphology-based phylogeny, Whalen and Landman (2022) position *D. syriaca* as a prototeuthid, the earliest diverging octobrachian clade. This fossil coleoid suborder possesses a slender, triangular-shaped gladius, which differs from the gladius shape of the other two fossil subgroups (Loligosepiina and Teudopseina) who have more developed lateral fields. Indeed, each of the 3 groups (Prototeuthina, Loligosepiina, and Teudopseina) bear a distinctive gladius that is generally homologous on a subordinal level, though displays considerable variation at a genus and species level (Fuchs 2016, 2020). Though this study documents previously unknown polymorphism in the gladius of *D. syriaca*, it is still consistent with the assignment to the prototeuthid.

**Lifestyle implications**.—The slender gladius morphology of *Dorateuthis syriaca* was originally compared with that of modern *Ommastrephes* d'Orbigny, 1835, by Woodward (1883) and has subsequently been explored by Fuchs and Iba (2015) and Bizikov and Toll (2016). The data presented here supports those comparisons and offers insight into the lifestyle of *D. syriaca*. Individuals of *Ommastrephes* spp. are powerful pelagic swimmers that are found in continental shelf environments and in nutrient-rich upwelling zones, preying on fish and crustaceans (Jereb and Roper 2010). Ommastrephidae Steenstrup, 1857, is a group of active visual hunters at all stages of ontogeny, generally fast growing, and vary in adult size based on relative growth rate in larval and juvenile stages (Jereb and Roper 2010).

The common muscular striations and elongated mantle indicate that *D. syriaca* also had the potential for active swimming. This would further be supported if the paired structures observed on the fossil individuals could be conclusively identified as head or funnel retractor musculature (Bizikov and Toll 2016; Fuchs et al. 2016a). The presence of prominent eyes suggest *D. syriaca* was a visual predator, and the volume and type of meal remains preserved in the digestive system indicates they were active feeders with a diet consisting largely of fish. The arms, differentiated in size, likely facilitated the manipulation of their relatively large prey, which would have needed to be disarticulated with their sharp beak before being ingested (Lukeneder and Harzhauser 2004; Nixon 2015); this feeding strategy is observed in Recent coleoids (Roscian et al. 2022). The expulsion of ink to conceal or confuse is a distinctive behaviour in modern forms (Bush and Robison 2007; Nixon 2011; Derby 2014) and ink sacs are preserved in almost all the individuals in the fossil sample. The size of the ink sac varies—though this is not interpreted as having a diagnostic value but rather reflects the amount of ink preserved in the organ (Fuchs 2006a). The presence of this character indicates they also utilized obfuscation techniques, likely to avoid predation.

# Conclusions

This study represents the most comprehensive analysis to date of *Dorateuthis syriaca* to combine non-destructive imaging techniques and comprehensive morphological measurements. The resulting qualitative and quantitative dataset provides the most comprehensive understanding to date of the morphology of this key species. The data allows us to rectify existing anatomical misinterpretations and character states from the published morphological matrix that were either previously unknown or coded incorrectly. It also highlights intraspecific anatomical variation related to ontogeny (e.g., arm length) or dimorphism (e.g., gladius morphology). Indeed, most individuals in the study are smaller than size ascribed for the genus diagnosis, and potentially represent juveniles or young adults. This emphasizes the need for a clearer understanding of the observed variation and whether this variation reflects ontogenetic stage.

In extant coleoids, a considerable amount of data on taxonomy, ecology, and lifestyle is determined by the configuration of soft tissues and internal organs. However, fossil coleoids are primarily known from their gladius. Though this structure is not often well preserved and difficult to classify, it dominates the purely palaeontological analyses of coleoid relationships. There is no complete soft tissue record for a species of Mesozoic Octobrachia, though the collective amount of data is growing. Exceptionally preserved coleoids from Lagerstätten deposits like Haqel, Hjoula, and Sahel Aalma, are vital in helping to bridge this divide as they retain evidence of soft tissues and provide unparalleled opportunities to study the anatomy and morphological detail of fossil coleoid groups.

The level of detail obtained in the present study shows the inherent benefits of using multimodal imagery to increase the quality of observations and, given the many

poorly resolved details in existing morphological matrices, emphasizes the need to re-evaluate a large number of specimens. However, diagenetic preservational processes are poorly understood in the Lebanese Lagerstätte deposits, making it difficult to establish a taphonomic model that can constrain pre-diagenetic decay, and thus morphological character loss. As such, identifying clear parameters to define the selectivity for preservation—what anatomical characters are likely to preserve and with what frequency—is now an essential step in the study of fossil coleoids for accurate character interpretation in any paleontological analysis from systematics to phylogenetic character coding or paleoecological interpretations.

# Acknowledgements

We thank SOLEIL synchrotron for provision of beamtime, Sebastian Schöder (SOLEIL synchrotron, Saint-Aubin, France) for assistance at the PUMA beamline, and IXRF, Austin, TX, USA for the provision of scan time and acquisition of elemental maps (proposal 20211554). We thank Olivier Béthoux (CR2P, Paris, France) for assistance with general RTI acquisition, and the acquisition of the RTI of the holotype of *D. syriaca*. We thank Robert Farrar (BHI, Hill City, South Dakota, USA), Didier Merle (MNHN, Paris, France), Zöe Hughes (NHMUK, London, UK) and Liath Appleton (NPL, Austin, Texas, USA) for collections assistance and sample loans. Additionally, to Sorbonne University students Aimie Doriath-Döhler and Robin Piguet-Ruinet (Paris, France) for their initial investigations on two specimens, MNHN.F.A88588 and MNHN.F.A88589 respectively, as part of an internship. We are also sincerely grateful to Alexandre Lethiers (CR2P) for the hypothesized reconstructions, and Lilian Cazes (CR2P) for photographs of the specimens. Finally, sincere thanks to Christian Klug (Paläontologisches Institut der Universität Zürich, Switzerland) and Arnaud Brayard (CNRS, Université de Bourgogne, Dijon, France) for their comments and revisions which greatly improved this manuscript. Part of this work was supported by the Paris Ile-de-France Region—DIM PAMIR-IDF-DIM-PAMIR-2023-4-028.

The authors report there are no competing interests to declare.

# References

Alfeld, M., Pedroso, J.V., Hommes van Eikema, M., Snickt, G, van der, Tauber, G., Blaas, J., Haschke, M., Erler, K., Dik, J., and Janssens, K. 2013. A mobile instrument for in situ scanning macro-XRF investigation of historical paintings. *Journal of Analytical Atomic Spectrometry* 28: 760–767.

Audo, D. and Charbonnier, S. 2012. New nisto of slipper lobster (Decapoda: Scyllaridae) from the Hadjoula Lagerstätte (Late Cretaceous, Lebanon). *Journal of Crustacean Biology* 32: 583–590.

Audo, D. and Charbonnier, S. 2013. Late Cretaceous crest-bearing shrimps from the Sahel Alma Lagerstätte of Lebanon. *Acta Palaeontologica Polonica* 58: 335–349.

Audo, D., Winkler, N., and Charbonnier, S. 2021. *Pseudodrobna natator* n. comb., a new link between crustacean faunas from the Jurassic of Germany and Cretaceous of Lebanon. *Geodiversitas* 43 (8): 209–218.

Bandel, K. and Leich, H. 1986. Jurassic Vampyromorpha (dibranchiate cephalopods). *Neues Jahrbuch für Geologie und Paläontologie Monatshefte* 1986 (3): 129–148.

Bather, F.A. 1888. Shell-growth in Cephalopoda (Siphonopoda). *Annals and Magazine of Natural History, Series 6* 1 (4): 298–310.

Béthoux, O., Llamosi, A., and Toussaint, S. 2016. Reinvestigation of *Protelytron permianum* (Insecta; Early Permian; USA) as an example for applying reflectance transformation imaging to insect imprint fossils. *Fossil Record* 20 (1): 1–7.

Binkhorst van den Binkhorst, J. 1861. *Monographie des Gastropodes et Céphalopodes de la Craie Supérieure du Limburg*. 44 pp. Verlag Muquart, Brüssel.

Bizikov, V.A. and Toll, R.B. 2016. Part M, Chapter 9A: The Gladius and its Vestiges in Extant Coleoidea. *Treatise Online* 77: 1–31.

Boyle, P. and Rodhouse, P. 2008. *Cephalopods: Ecology and Fisheries*. 452 pp. John Wiley & Sons, Oxford.

Bracchi, G. and Alessandrello, A. 2005. *Paleodiversity of the Free-living Polychaetes:(Annelida, Polychaeta) and Description of New Taxa from the Upper Cretaceous Lagerstätten of Haqel, Hadjula and Al-Namoura (Lebanon)*. 64 pp. Società Italiana di Scienze Naturali e Museo Civico di Storia Naturale di Milano, Milan.

Bush, S. and Robison, B. 2007. Ink utilization by mesopelagic squid. *Marine Biology* 152: 485–494.

Charbonnier, S. 2009. Le Lagerstätte de La Voulte: un environnement bathyal au Jurassique. *Mémoires du Muséum national d'Histoire naturelle* 199: 1–272.

Charbonnier, S., Audo, D., Caze, B., and Biot, V. 2014. The La Voulte-sur-Rhône Lagerstätte (Middle Jurassic, France). *Comptes Rendus Palevol* 13: 369–381.

Charbonnier, S., Audo, D., Garassino, A., and Hyžný M. 2017. Fossil Crustacea of Lebanon. *Mémoires du Muséum national d'Histoire naturelle* 210: 1–252.

Chun, C. 1903. *Aus den Tiefen des Weltmeeres*. 592 pp. Gustav Fischer, Jena.

Clements, T. and Gabbott, S. 2022. Exceptional preservation of fossil soft tissues. *eLS* 2: 1–10.

Clements, T., Colleary, C., De Baets, K., and Vinther, J. 2017. Buoyancy mechanisms limit preservation of coleoid cephalopod soft tissues in Mesozoic Lagerstätten. *Palaeontology* 60: 1–14.

Clements, T., Purnell, M.A., and Gabbott, S. 2022. Experimental analysis of organ decay and pH gradients within a carcass and the implications for phosphatization of soft tissues. *Palaeontology* 65 (4): e12617.

Derby, C.D. 2014. Cephalopod ink: production, chemistry, functions and applications. *Marine Drugs* 12: 2700–2730.

Donovan, D.T. and Fuchs, D. 2016. Part M, Chapter 13: Fossilized Soft Tissues in Coleoidea. *Treatise Online* 73: 1–30.

d' Orbigny, A.D. 1835. *Voyage dans l'Amérique méridionale (le Brésil, la république orientale de l'Uruguay, la République argentine, la Patagonie, la république du Chili, la république de Bolivia, la république du Pérou), exécuté pendant les années 1826, 1827, 1828, 1829, 1830, 1831, 1832 et 1833. Mollusques. Première Classe. Céphalopodes, Cephalopoda. (Cuvier, Etc.)*. 64 pp. P. Bertrand, Paris.

Ejel, F. and Dubertret, L. 1966. On the precise age of the Cretaceous fish and crustacean deposit of Sahel Alma (Lebanon). *Summary Report of the Sessions of the Geological Society of France* 9: 353–354.

El Hossny, T. and Cavin, L. 2023. A new enigmatic teleost fish from the Mid-Cretaceous of Lebanon. *Diversity* 15 (7): 839.

Engeser, T. 1988. Vampyromorpha ("Fossile Teuthiden"). *In*: F. Westphal (ed.), *Fossilium Catalogus. Animalia Vol. 130*, 1–167. Kugler Publications, Amsterdam.

Engeser, T. and Reitner, J. 1985. Teuthiden aus dem Unterapt ("Töck") von Helgoland (Schleswig-Holstein, Norddeutschland): Teuthids from the Early Aptian ("Töck") of Heligoland (Schleswig-Holstein, North Germany). *Paläontologische Zeitschrift* 59: 245–260.

Engeser, T. and Reitner, J. 1986. Coleoidenreste aus der Oberkreide des Libanon im Staatlichen Museum für Naturkunde in Stuttgart. *Stuttgarter Beiträge zur Naturkunde: Serie B Geologie und Paläontologie* 124: 1–17.

Ferry, S., Merran, Y., Grosheny, D., and Mroueh, M. 2007. The Cretaceous of Lebanon in the Middle East (levant) context. *In*: L.G. Bulot, S. Ferry, and D. Grosheny (eds.), Relations entre les marges septen-

trionale et méridionale de la Téthys au Crétacé. *Carnets de Géologie* (CG2007_M02/08): 38–42.

Fischer, J.-C. and Riou, B. 1982. Les teuthoïdes (Cephalopoda, Dibranchiata) du Callovien inférieur de la Voulte-sur-Rhône (Ardèche, France). *Annales de Paléontologie* 68: 295–325.

Fischer, J.-C. and Riou, B. 2002. *Vampyronassa rhodanica* nov. gen. nov. sp., vampyromorphe (Cephalopoda, Coleoidea) du Callovien inférieur de la Voulte-sur-Rhône (Ardèche, France). *Annales de Paléontologie* 88: 1–17.

Forey, P.L., Yi, L., Patterson, C., and Davies, C.E. 2003. Fossil fishes from the Cenomanian (Upper Cretaceous) of Namoura, Lebanon. *Journal of Systematic Palaeontology* 1: 227–330.

Fraas, O. 1878. Geologisches aus dem Libanon. *Jahreshefte des Vereins für vaterländische Naturkunde in Württemberg.* 34: 257–391.

Fuchs, D. 2006a. Fossil erhaltungsfahige Merkmalskomplexe der Coleoidea (Cephalopoda) und ihre phylogenetische Bedeutung. *Berliner paläobiologische Abhandlungen* 8: 1–122.

Fuchs, D. 2006b. Morphology, taxonomy and diversity of vampyropod coleoids (Cephalopoda) from the Upper Cretaceous of Lebanon. *Memorie della Società italiana di Scienze naturali e del Museo civico di Storia naturale di Milano* 34: 1–28.

Fuchs, D. 2007. Coleoid cephalopods from the plattenkalks of the Upper Jurassic of Southern Germany and from the Upper Cretaceous of Lebanon: A faunal comparison. *Neues Jahrbuch für Geologie und Paläontologie Abhandlungen* 245: 59–69.

Fuchs, D. 2016. Part M, Chapter 9B: The Gladius and Gladius Vestige in Fossil Coleoidea. *Treatise Online* 83: 23 pp.

Fuchs, D. 2020. Part M, Chapter 23G: Systematic Descriptions: Octobrachia. *Treatise Online* 138: 1–52.

Fuchs, D. and Iba, Y. 2015. The gladiuses in coleoid cephalopods: homology, parallelism, or convergence? *Swiss Journal of Palaeontology* 134: 187–197.

Fuchs, D. and Larson, N. 2011a. Diversity, morphology, and phylogeny of coleoid cephalopods from the Upper Cretaceous Plattenkalks of Lebanon—Part I: Prototeuthidina. *Journal of Paleontology* 85: 234–249.

Fuchs, D. and Larson, N. 2011b. Diversity, morphology, and phylogeny of coleoid cephalopods from the Upper Cretaceous Plattenkalks of Lebanon—Part II: Teudopseina. *Journal of Paleontology* 85: 815–834.

Fuchs, D. and Weis, R. 2009. A new Cenomanian (Late Cretaceous) coleoid (Cephalopoda) from Hâdjoula, Lebanon. *Fossil Record* 12: 175–181.

Fuchs, D., Bracchi, G., and Weis, R. 2009. New Octopods (Cephalopoda: Coleoidea) from the Late Cretaceous (Upper Cenomanian) of Häkel and Hädjoula, Lebanon. *Palaeontology* 52: 65–81.

Fuchs, D., Engeser, T., and Keupp, H. 2007a. Gladius shape variation in coleoid cephalopod *Trachyteuthis* from the Upper Jurassic Nusplingen and Solnhofen Plattenkalks. *Acta Palaeontologica Polonica* 52: 575–589.

Fuchs, D., Iba, Y., Tischlinger, H., Keupp, H., and Klug, C. 2016a. The locomotion system of Mesozoic Coleoidea (Cephalopoda) and its phylogenetic significance. *Lethaia* 49: 433–454.

Fuchs, D., Keupp, H., and Schweigert, G. 2013. First record of a complete arm crown of the Early Jurassic coleoid *Loligosepia* (Cephalopoda). *Paläontologische Zeitschrift* 87: 431–435.

Fuchs, D., Klinghammer, A., and Keupp, H. 2007b. Taxonomy, morphology and phylogeny of plesioteuthidid coleoids from the Upper Jurassic (Tithonian) Plattenkalks of Solnhofen. *Neues Jahrbuch für Geologie und Paläontologie Abhandlungen* 245: 239–252.

Fuchs, D., Wilby, P.R., von Boletzky, S., Abi-Saad, P., Keupp, H., and Iba, Y. 2016b. A nearly complete respiratory, circulatory, and excretory system preserved in small Late Cretaceous octopods (Cephalopoda) from Lebanon. *PalZ* 90: 299–305.

George, H., Bazzi, M., El Hossny, T., Ashraf, N., Abi Saad, P., Clements, T. 2024. The famous fish beds of Lebanon: the Upper Cretaceous Lagerstätten of Haqel, Hjoula, Nammoura, and Sahel Aalma. *Journal of the Geological Society* 181 (5): jgs 2023-210.

Grimpe, G. 1916. *Chunioteuthis*: eine neue Cephalopodengattung. *Zoologischer Anzeiger* 46: 349–359.

Gueriau, P., Jauvion, C., and Mocuta, C. 2018. Show me your yttrium, and I will tell you who you are: implications for fossil imaging. *Palaeontology* 61: 981–990.

Haeckel, E.H.P.A. 1866. *Generelle Morphologie Der Organismen. Allgemeine Grundzüge Der Organischen Formen-Wissenschaft, Mechanisch Begründet Durch Die von Charles Darwin Reformirte Descendenztheorie, von Ernst Haeckel*. 617 pp. G. Reimer, Berlin.

Hanlon, R., Vecchione, M., and Allcock, L. 2018. *Octopus, Squid, and Cuttlefish: A Visual, Scientific Guide to the Oceans' Most Advanced Invertebrates*. 223 pp. University of Chicago Press, Chicago.

Hart, M.B., Page, K.N., Price, G.D., and Smart, C. W. 2019. Reconstructing the Christian Malford ecosystem in the Oxford Clay Formation (Callovian, Jurassic) of Wiltshire: exceptional preservation, taphonomy, burial and compaction. *Journal of Micropalaeontology* 38: 133–142.

Jattiot, R., Brayard, A., Fara, E., and Charbonnier, S. 2015. Gladius-bearing coleoids from the Upper Cretaceous Lebanese Lagerstätten: Diversity, morphology, and phylogenetic implications. *Journal of Paleontology* 89: 148–167.

Jereb, P. and Roper, C.F.E. (eds.) 2010. *Cephalopods of the World: An Annotated and Illustrated Catalogue of Cephalopod Species Known to Date. Vol. 2. Myopsid and Oegopsid Squids*. *FAO Species Catalogue for Fishery Purposes*, no. 4. 605 pp. Food and Agriculture Organization of the United Nations, Rome.

Klinghardt, F. 1943. Vergleichende untersuchungen über tintenfische und belemnitenähnliche weichtiere. *Sitzungsberichte der Gesellschaft naturforschender Freunde in Berlin* 1942: 5–17.

Klug, C., Di Silvestro, G., Hoffmann, R., Schweigert, G., Fuchs, D., Clements, T., and Gueriau, P. 2021c. Taphonomic patterns mimic biologic structures: diagenetic Liesegang rings in Mesozoic coleoids and coprolites. *PeerJ* 9: e10703.

Klug, C., Fuchs, D., Schweigert, G., Röper, M., and Tischlinger, H. 2015. New anatomical information on arms and fins from exceptionally preserved *Plesioteuthis* (Coleoidea) from the Late Jurassic of Germany. *Swiss Journal of Palaeontology* 134: 245–255.

Klug, C., Hoffmann, R., Tischlinger, H., Fuchs, D., Pohle, A., Rowe, A., Rouget, I., and Kruta, I. 2023. "Arm brains" (axial nerves) of Jurassic coleoids and the evolution of coleoid neuroanatomy. *Swiss Journal of Palaeontology* 142: 1–22.

Klug, C., Pohle, A., Roth, R., Hoffmann, R., Wani, R., and Tajika, A. 2021b. Preservation of nautilid soft parts inside and outside the conch interpreted as central nervous system, eyes, and renal concrements from the Lebanese Cenomanian. *Swiss Journal of Palaeontology* 140: 1–11.

Klug, C., Schweigert, G., Dietl, G., and Fuchs, D. 2005. Coleoid beaks from the Nusplingen Lithographic Limestone (Upper Kimmeridgian, SW Germany). *Lethaia* 38: 173–192.

Klug, C., Schweigert, G., Fuchs, D., and De Baets, K. 2021a. Distraction sinking and fossilized coleoid predatory behaviour from the German Early Jurassic. *Swiss Journal of Palaeontology* 140: 1–12.

Kolbe, H. 1888. Zur Kenntniss von Insektenbohrgängen in fossilen Hölzern. *Zeitschrift der deutschen geologischen Gesellschaft* 40: 131–137.

Kruta, I., Rouget, I., Charbonnier, S., Bardin, J., Fernandez, V., Germain, D., Brayard, A., and Landman, N. 2016. *Proteroctopus ribeti* in coleoid evolution. *Palaeontology* 59: 767–773.

Leclercq, N., Berthault, J., Langlois, F., Lê, S., Poirier, S., Bisou, J., Blache, F., Medjoubi, K., and Mocuta, C. 2015. flyScan: A Fast and Multi-Technique Data Acquisition Platform for the SOLEIL Beamlines. *In*: L. Corvetti, K. Riches, and V.R.W. Schaa (eds.), *Proceedings of the 15th International Conference on Acelerator and Large Experimental Physics Control Systems-ICALEPCS*, 826–829. JACoW, Geneva.

Lehmann, J., Bornemann, A., Jattiot, R., Nohra, R., and Resch, U. 2024. Age constraint of the Cenomanian (Late Cretaceous) Fossillagerstätte of Hjoûla (Lebanon) based on ammonites. *Newsletters on Stratigraphy* 57: 203–223.

Lindgren, A.R., Giribet, G., and Nishiguchi, M.K. 2004. A combined approach to the phylogeny of Cephalopoda (Mollusca). *Cladistics* 20: 454–486.

Lukeneder, A. and Harzhauser, M. 2004. The Cretaceous coleoid *Dorateuthis syriaca* Woodward: morphology, feeding habits and phylogenetic implications. *Annalen des Naturhistorischen Museums in Wien. Serie A für Mineralogie und Petrographie, Geologie und Paläontologie, Anthropologie und Prähistorie* 106: 213–225.

Mangold, K.M. and Young, R.E. 1998. The systematic value of the digestive organs. *Smithsonian Contributions to Zoology* 586: 21–30.

Marroquín, S.M., Martindale, R.C., and Fuchs, D. 2018. New records of the late Pliensbachian to early Toarcian (Early Jurassic) gladius-bearing coleoid cephalopods from the Ya Ha Tinda Lagerstätte, Canada. *Papers in Palaeontology* 4: 245–276.

Martindale, R.C., Them, T.R., Gill, B.C., Marroquín, S.M., and Knoll, A.H. 2017. A new Early Jurassic (ca. 183 Ma) fossil *Lagerstätte* from Ya Ha Tinda, Alberta, Canada. *Geology* 45: 255–258.

Muscente, A.D., Martindale, R.C., Schiffbauer, J.D., Creighton, A.L., and Bogan, B.A. 2019. Taphonomy of the Lower Jurassic Konservat-Lagerstätte at Ya Ha Tinda (Alberta, Canada) and its significance for exceptional fossil preservation during oceanic anoxic events. *Palaios* 34: 515–541.

Naef, A. 1921. Das System der dibranchiaten Cephalopoden und die mediterranen Arten derselben. *Mitteilungen aus der zoologischen Station zu Neapel* 22: 527–542.

Naef, A. 1922. *Die fossilen Tintenfische: eine paläozoologische Monographie*. 322 pp. Verlag von Gustav Fischer, Jena.

Nixon, M. 2011. Part M, Chapter 3: Anatomy of Recent forms. *Treatise Online* 17: 1–49.

Nixon, M. 2015. Part M, Chapter 12: The Buccal Apparatus of Recent and Fossil Forms. *Treatise Online* 69: 1–30.

Purnell, M.A., Donoghue, P.J., Gabbott, S.E., McNamara, M.E., Murdock, D.J., and Sansom, R.S. 2018. Experimental analysis of soft-tissue fossilization: opening the black box. *Palaeontology* 61: 317–323.

Reich, M. 2004. Holothurians from the Late Cretaceous "Fish shales" of Lebanon. *In*: T. Heinzeller and J. Nebelsick (eds.), *Echinoderms: Proceedings of the 11th International Echinoderm Conference, Munich, Germany*, 487–488. Taylor & Francis Group, London.

Reitner, J. and Engeser, T. 1982. Teuthiden aus dem Barrême der Insel Maio (Kapverdische Inseln). *Paläontologische Zeitschrift* 56: 209–216.

Riegraf, W. 1987. *Plesioteuthis arcuata* von der Marck 1873 (Cephalopoda, Teuthida) from the Campanian (late Cretaceous) of Westfalia (NW Germany). *Münstersche Forschungen zur Geologie und Paläontologie* 66: 95–110.

Roger, J. 1946. Les invertébrés des couches à poisons du crétace supérieur du Liban: *Mémoires de la Société Géologique de France. Nouvelle Série* 51: 1–92.

Roger, J. 1952. Sous-classe des Dibranchiata Owen 1836. *In*: J. Piveteau (ed.), *Traité de Paléontologie Vol. 2*, 689–755. Masson, Paris.

Roscian, M., Herrel, A., Zaharias, P., Cornette, R., Fernandez, V., Kruta, I., Cherel, Y., and Rouget, I. 2022. Every hooked beak is maintained by a prey: Ecological signal in cephalopod beak shape. *Functional Ecology* 36: 2015–2028.

Rowe, A.J., Kruta, I., Landman, N.H., Villier, L., Fernandez, V., and Rouget, I. 2022. Exceptional soft-tissue preservation of Jurassic *Vampyronassa rhodanica* provides new insights on the evolution and palaeoecology of vampyroteuthids. *Scientific Reports* 12: 1–9.

Rowe, A.J., Kruta, I., Villier, L., and Rouget, I. 2023. A new vampyromorph species from the Middle Jurassic La Voulte-sur-Rhône Lagerstätte. *Papers in Palaeontology* 9 (3): p.e1511.

Rüppell, E. 1829. *Abbildung und Beschreibung einiger neuen oder wenig gekannten Versteinerungen aus der Kalkschieferformation von Solenhofen*. 12 pp. Verlag der Brönner'schen buchhandlung, (S. Schmerber), Frankfurt a. M.

Schindelin, J., Arganda-Carreras, I., Frise, E., Kaynig, V., Longair, M., Pietzsch, T., Preibisch, S., Rueden, C., Saalfeld, S., and Schmid, B. 2012. Fiji: an open-source platform for biological-image analysis. *Nature Methods* 9: 676–682.

Solé, V.A., Papillon, E., Cotte, M., Walter, P., and Susini, J. 2007. A multiplatform code for the analysis of energy-dispersive X-ray fluorescence spectra. *Spectrochimica Acta Part B: Atomic Spectroscopy* 62: 63–68.

Steenstrup 1857. Oplysning om en ny Art af Blaeksprutter. *Oversigt over det Kongelige Danske Videnskabernes Selskabs Forhandlinger* 1857 (1/2): 11–14.

Sutton, M., Perales-Raya, C., and Gilbert, I. 2016. A phylogeny of fossil and living neocoleoid cephalopods. *Cladistics* 32: 297–307.

Swinburne, N.H. and Hemleben, C. 1994. The plattenkalk facies: A deposit of several environments. *Geobios* 27: 313–320.

Toll, R.B. 1988. Functional morphology and adaptive patterns of the teuthoid gladius. *In*: K.M Wilbur (ed.), *The Mollusca*, 167–182. Academic Press, Orlando.

von der Marck, W. 1873. Neue Beiträge zur Kenntnis der fossilen Fische und anderer Thierreste aus der jüngsten Kreide Westfalens. *Palaeontographica* 22: 55–74.

Wells, M.J. 2011. Part M, Chapter 4: Physiology of Coleoids. *Treatise Online* 27: 1–39.

Whalen, C.D. and Landman, N.H. 2022. Fossil coleoid cephalopod from the Mississippian Bear Gulch Lagerstätte sheds light on early vampyropod evolution. *Nature Communications* 13 (1): 1107.

Wilby, P., Hudson, J., Clements, R., and Hollingworth, N. 2004. Taphonomy and origin of an accumulate of soft-bodied cephalopods in the Oxford Clay Formation (Jurassic, England). *Palaeontology* 47: 1159–1180.

Wippich, M.G.E. and Lehmann, J. 2004. *Allocrioceras* from the Cenomanian (mid-Cretaceous) of the Lebanon and its bearing on the palaeobiological interpretation of heteromorphic ammonites. *Palaeontology* 47: 1093–1107.

Woodward, H. 1883. I. On a new genus of fossil "Calamary", from the Cretaceous Formation of Sahel Alma, near Beirût, Lebanon, Syria. *Geological Magazine* 10: 1–5.

Woodward, H. 1896. On a fossil octopus (Calais Newboldi, J. De C. Sby. MS.) from the Cretaceous of the Lebanon. *Quarterly Journal of the Geological Society* 52: 229-NP.

Young, R.E. and Vecchione, M. 1996. Analysis of morphology to determine primary sister-taxon relationships within coleoid cephalopods. *American Malacological Bulletin* 12: 91–112.

Young, R.E., Vecchione, M., and Mangold, K.M. 2001. *Cephalopod Fin Position*. The Tree of Life Web Project [downloaded from http://tolweb.org/accessory/Cephalopod_Fin_Position?acc_id=2041#AboutThisPage on 26 August 2023].